PRODUCT-SPECIFIC KINETICS REVEAL EFFECT OF EPOXY CRYSTALLIZATION ON THERMOSET THERMAL DEGRADATION

Derek B. Dwyer, Nidia Gallego, Sara Isbill, Andrew Miskowiec, J. L. Niedziela*

Oak Ridge National Laboratory, P.O. Box 2008 MS-6117, Oak Ridge, TN

*Corresponding author: dwyerdb@ornl.gov

KEYWORDS. Crystallized epoxy resin, thermoset, EGA-MS, product-specific kinetics, bisphenol F

ABSTRACT

Crystallization is a common problem for epoxy resins, which are ubiquitous in industrial and commercial use. Integration of crystalized epoxy monomers into cured thermosets has been shown to alter the thermosets' final mechanical properties. However, no studies have investigated

the impact of these crystals on the thermal stability of the thermoset. Here we investigate the degradation kinetics of a bisphenol F–based epoxy thermoset with and without crystalized monomers using Product-Specific Kinetic (PSK) analysis coupled with Evolved Gas Analysis-Mass Spectrometry (EGA-MS). PSK analysis revealed significant differences in evolved product ion kinetics, suggesting changes in the degradation kinetics between thermoset configurations. It was concluded that early stages of degradation are influenced most by crystal presence due to the high concentration of unreacted epoxy monomers and lower cross-linking density of the cured network. After post-cure annealing, significant changes are observed in the degradation kinetics of thermosets without crystal inclusions. Conversely, post-cure annealing procedures of crystal integrated thermosets showed little change in the thermoset degradation kinetics across all conversion extents. These findings suggest that post-cure annealing of thermosets with crystals present at the onset does not alter the cross-linking density of the polymer network enough to significantly change the degradation kinetics. We hypothesize this is because the excess monomers from the melted crystals are unable to find suitable reaction sites for complete binding into the polymer network, which has direct implications for the material properties and final thermal stability of the thermoset.

1. Introduction

Epoxy thermosets are highly cross-linked polymer materials that serve as the binding polymer matrix in reinforced carbon fiber composites. The carbon fiber components have higher thermal tolerance, with the maximum temperatures for the fibers themselves generally aligned with final firing temperature used in the fiber production process, when heated in inert conditions.[1-4] However after addition of the polymer thermoset, the thermal resilience of the final composite is limited by the heat tolerance of the polymer.[5] Consequently, an understanding of the thermal

degradation mechanisms and kinetics of these epoxy thermosets are desired to fully understand the response of carbon composites to conditions involving high heat and thermal exposure. Numerous works have investigated the degradation mechanisms of epoxy thermosets[6-9] and, to a lesser extent, degradation kinetics.[10, 11] More have investigated the impact of integrated filler or blended components in the thermoset on its thermal stability. [12-16]

A well-known but understudied phenomena of epoxy thermosets is epoxy monomer crystallization. Epoxy crystallization is a common process in epoxy resins, and the degree to which crystallization may influence thermal degradation and stability is an open question. Epoxy resins are considered supercooled fluids. The supercooled state leads to epoxy resins generally being a viscous liquid at room temperature despite having melting points above room temperature (45–48 °C).[17, 18] This delicate state renders them prone to crystallization during prolonged storage, temperature fluctuations, or exposure to contaminants. Crystallization in resin precursors may be detected at point of use and removed through heating. However, crystallization not detected due to small size of crystal can be included in the final composite, resulting in unexpected failures, mechanical instability, or reduced thermal performance.

Investigations of crystallization in epoxy thermosets is limited to alterations to the mechanical properties of thermosets integrated with epoxy crystals.[19] Separately, there have been related studies using liquid-crystal thermosets investigating the impact of crystal integration on thermoset thermal stability. These studies involved direct integration of liquid-crystal epoxy monomers into the polymer network structure which subsequently form crystalline domains within the network. The results conflict, with some studies showing improvements in thermal stability of the thermoset with other studies showing no impact on thermal stability.[20-22]

However, there have been no investigations of the effects from integration of crystallized epoxy monomers on the thermosets' thermal stability and degradation kinetics. Integration of crystallized epoxy monomers into the thermoset polymer network is notably different than analogous liquid-crystal systems. In crystallized epoxy monomers, the crystalline regions are not chemically bound to the polymer network. This leaves a complex multistep process upon heating from crystal melt, monomer diffusion, void formation, to final reaction of the monomers with the formed polymer network all of which could impact the thermal stability of the final thermoset.

Previously, Product-Specific Kinetic (PSK) analysis coupled with Evolved Gas Analysis-Mass Spectrometry (EGA-MS) differentiated kinetic values, specifically activation energy (E_a), between degradation products produced simultaneously during the thermal degradation of bisphenol F based epoxy thermoset.[10] The *Kissinger* method was utilized to determine both activation energy and Arrhenius pre-exponential factor of specific degradation products using PSK. However, the peak temperature method used is blind to the changes that occur in the E_a over the entirety of the degradation process. Conversely, isoconversional kinetics monitors the change in kinetics over the entirety of degradation, allowing for a more detailed analysis of the data.

There are several publications with in depth discussions of isoconversional analysis, specifically works by S. Vyazovkin.[10, 23-28] In short, isoconversional analysis are nonisothermal methods that provide an apparent activation energy derived from the fraction of the overall change in a physical property being measured, also known as the extent of conversion (α).[10, 23] Apparent activation energy is the accumulation of individual and simultaneous reactions providing important information regarding the degradation process of the system. In the case of PSK, the apparent activation energy is hypothesized to represent the activation energy of the specific reaction being monitored.[10] Therefore, changes in the apparent activation energy are associated with differences

in the specific product mechanism and can provide a higher level of detail then non-PSK based methods, especially when combined with isoconversional analysis.

In this current work, EGA-MS, isoconversional analysis, and PSK are used to elucidate differences that arise in the degradation kinetics of compositionally identical epoxy thermosets based on bisphenol F epoxy with and without integration of crystalized epoxy monomers. Bisphenol F epoxy is used in the construction of plastics and resins, including structural components, thus understanding the thermal degradation and kinetics of this material is crucial to building safety. Further, bisphenol F is structurally related to bisphenol A, and sought as a replacement for bisphenol A epoxies due to concern over hormone disruption and related health effects demonstrated for bisphenol A based plastics.[29]

2. Methods

2.1 Materials

A bisphenol F–based epoxy resin (Araldite PY306 US) was obtained from Huntsman and used without further purification. Trimethylolpropane tris[poly(propylene glycol), amine terminated] ether (T-403) was received from Sigma-Aldrich and used without further purification.

2.2 Thermoset Synthesis

Thermosets were prepared by first preheating the PY306 epoxy resin at 358 K for 1 h to melt any formed crystals. Then, 1.002 g and 0.900 g of PY306 resin were weighed into two separate disposable beakers. Next, 449 μL of T-403 hardener was added separately to both samples and mixed by hand. Prepolymer formulations were degassed at 358 K. Finally, 102 mg of crystalized PY306 resin was added to the 0.900 g epoxy sample after cooling and mixed thoroughly to create a 10% by weight of epoxy resin in the sample, designated as PY306/T-403 10% (PT10). However, due to some of the epoxy crystal reacting with the forming polymer matrix,[19] the true weight

percentage of epoxy crystal to epoxy resin is less than 10%. Both the PT10 and PY306/T-403 (PT) prepolymer formulations had 2:1 molar equivolents of epoxy to amine functional groups and were cured at room temperature for 72 h before analysis. After preliminary analysis, samples underwent a final post cure anneal at 358 K for 17 hrs. Powdered samples for kinetic analysis were prepared using a Polymer Prepper grinding tool (Frontier Laboratories Ltd.).

2.3 Polarized Optical Microscopy

A Nikon eclipse LV100N POL microscope coupled to a Linkam THMS600 heating stage was used for in situ heating experiments using POM. All images were taken under transmitted light. A heating rate of 5 °C/min was used.

2.4 Evolved Gas Analysis-Mass Spectrometry

EGA-MS experiments were performed in helium using a multishot pyrolyzer (PY-3030D, Frontier Analytical Ltd.) interfaced with an Agilent GC (7890B)-MSD (5977A) with a carrier gas selector (CGS-1050Ex), a selective sampler (SS-1010E), and an Auto-Shot (AS-1020E) from Frontier Analytical Ltd. A deactivated Ultra ALLOY EGA tube (UADTM-2.5N) was used (2.5 m length, 0.15 mm inner diameter, and 0.47 mm outer diameter). The following inlet parameters were used for analysis: the heater was set at 553 K and had a total flow of 139.4 mL/min. The pressure was set to 171.8 kPa, and the heater had a septum purge flow of 3 mL/min and a split flow of 135.2 mL/min. The gas chromatography oven was set at 573 K, and the column settings were a flow of 1.2 mL/min, pressure of 171.8 kPa, average velocity of 43.8 cm/s, and hold time of 1.1 min. The mass spectra scan range was set to monitor ions *m/z* 29–400. Separate experiments were performed using the selected ion monitoring (SIM) mode, which was set to monitor ions *m/z* 66, *m/z* 182, and *m/z* 200. These ions were selected because *m/z* 66, *m/z* 182, and *m/z* 200 are unique ions for phenol, xanthene, and bisphenol F isomers, respectively, which are major

degradation products for bisphenol F thermoset.[10] An electron impact voltage of 70 eV was used in all experiments. Furnace calibrations are described elsewhere.[10] Powdered samples were prepared in 80 μL stainless steel Eco-cups™ from Frontier with sample masses ranging from 100 to 230 μg. Thermal exposures were conducted with a 1 min hold at 313 K before heating at a rate of 5, 10, or 20 K/min up to 973 K, followed by a final 1 min hold. Three trials were performed for each experiment with standard uncertainties (u) presented in the results.

2.5 Thermogravimetric Analysis

Thermogravimetric analysis was performed using a TA Instruments Q5000 TGA system under N_2 atmosphere with standard gas flow rate of 50 mL/min. Powdered samples of approximately 5 mg were loaded into a high-temperature platinum pan after tare. Samples were heated at heating rates of 5, 10, and 20 K/min up to 973 K and held at temperature for 1 min. Two experiments were performed for each heating rate.

2.6 Kinetic Analysis

An isoconversional kinetic method was used to determine the apparent activation energy for the epoxy thermoset degradation. First, extent conversion plots were prepared from the total and extracted ion thermographs (EITs) using eq 1.

$$\mathrm{A} = \frac{AMI_T}{AMI_f} \tag{1}$$

where AMI_T is the accumulated mass intensity at a given temperature T, AMI_f is the accumulated mass intensity at the final temperature, and α is the extent of conversion.[30] Extent conversion plots from thermogravimetric analysis data are obtained from eq 2:

$$\alpha = \frac{m_o - m}{m_o - m_f} \tag{2}$$

where m_o and m_f are the initial and final masses, respectively. The activation energy, E_a, was calculated at arbitrarily selected conversions using a modified form of the Kissinger–Akahira–Sunose equation, eq 3.[24, 31]

$$\ln\frac{\beta_i}{T^B_{\alpha,i}} = Const - C \times \frac{E_a}{RT_{\alpha,i}} \quad (3)$$

where β_i is the heating rate, $T_{\alpha,I}$ is the temperature at a specific α and heating rate, R is the universal gas constant, B = 2, and C = 1. Equation 3 was modified by Starink, who showed E_a can be estimated more accurately by substituting B with 1.92 and C with 1.0008 to yield eq 4.[32]

$$\ln\frac{\beta_i}{T^{1.92}_{\alpha,i}} = Const - 1.0008 \times \frac{E_a}{RT_{\alpha,i}} \quad (4)$$

The activation energy was then calculated from the slope of $\ln(\beta_i/T^{1.92}_{\alpha,i})$ against $1/T_{\alpha,i}$.

2.7 Computation

Carbon-oxygen bond energies were calculated for an amine-terminated bisphenol A epoxy monomer using the NWChem 6.8 electronic structure theory package[33] on the Compute and Data Environment for Science (CADES) cluster at Oak Ridge National Laboratory. The M06-2X exchange-correlation functional[34] was combined with the cc-pVDZ basis set[35] and Grimme's D3 van der Waals corrections[36] to describe the interatomic interactions, consistent with our previous work.[37] Forces were minimized until the default convergence tolerances were reached.

3. Results and Discussion

3.1 Bisphenol F Epoxy Structure and Crystal Integration

The ideal chemical structures of the PY306 epoxy resin and T-403 hardener are shown in Figure 1. This resin contains an isomeric mixture of bisphenol F epoxy resins which has been reported previously in the literature.[38] Epoxy crystals were present upon receiving the resin and were

removed via mild heating at 358 K for 24 hrs. Crystals were observed to reform after prolonged storage of approximately 4 months.

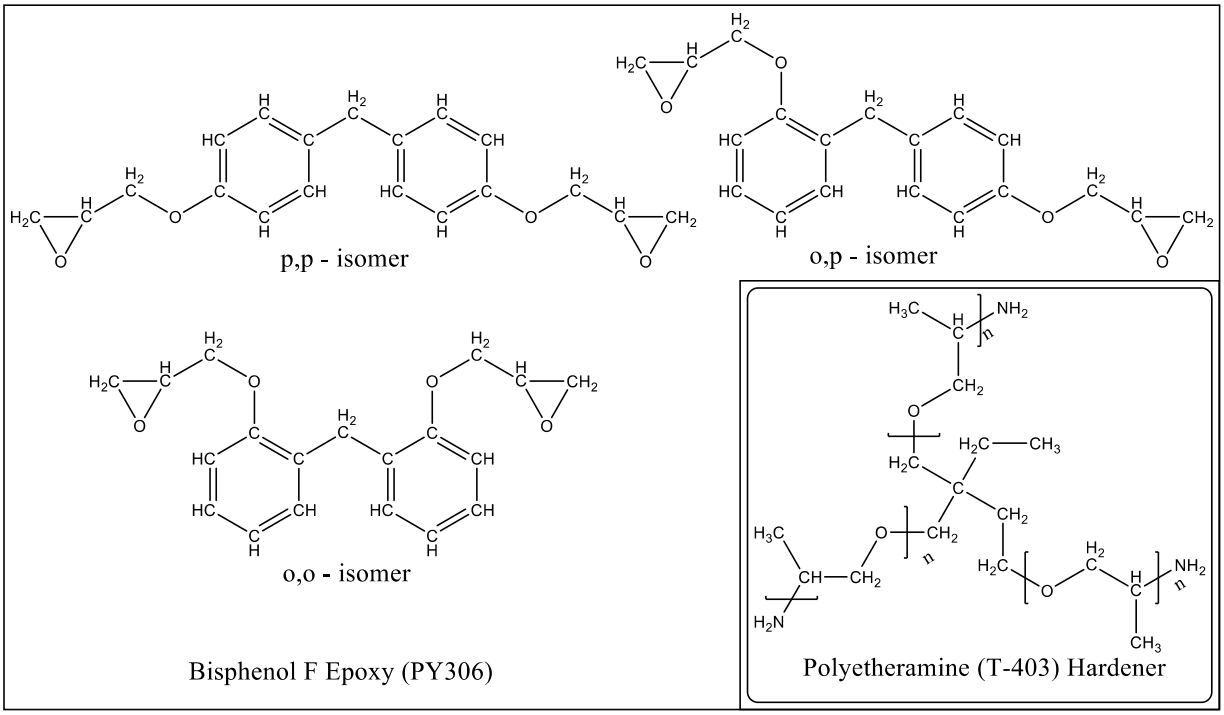

Figure 1. Chemical structure of PY306 epoxy resin showing three isomers present in the resin and the chemical structure of T-403 hardener.

Formation of crystals in the prepolymer epoxy resins manifests as cloudiness with continued growth of crystals eventually leading to complete solidification. Images of the crystalized epoxy resin and crystal integrated thermoset are shown in Figure 2 along with the liquid epoxy resin and thermoset without crystals. Crystals in the final thermoset are visibly apparent as cloudiness in the material.

Figure 2. Picture of liquid and crystalized epoxy resin and cured thermoset with and without integrated epoxy crystals. Crystalized epoxy resin and crystal integrated thermosets are marked with red arrows.

The degradation kinetics of room temperature cured (PT and PT10) and post cure annealed (PT [PC] and PT10 [PC]) thermosets were investigated in this work. Post cure annealing procedures are performed to hypothetically achieve higher curing completion by increasing cross-linking density. In the present work, two different starting conditions of the PT10 thermoset are used. After a room temperature cure, PT10 thermosets contain embedded epoxy crystals which are identified by cloudiness in the thermoset. Due to their anisotropy, epoxy crystals display birefringence under double polarized light, allowing them to be easily detected using polarized optical microsopy (POM), Figure 3A. When heated above their melting point, the crystals melt resulting in loss of birefringence and formation of a resin filled pocket. With further heating, the epoxy monomers diffuse into the polymer network causing strain to form at the interface between the polymer network and the void interface. The increasing polymer strain causes a corresponding increase in strain birefringence evident in POM, Figure 3B.[19] The transition from crystal to strain birefringence is summarized in Figure 3C.

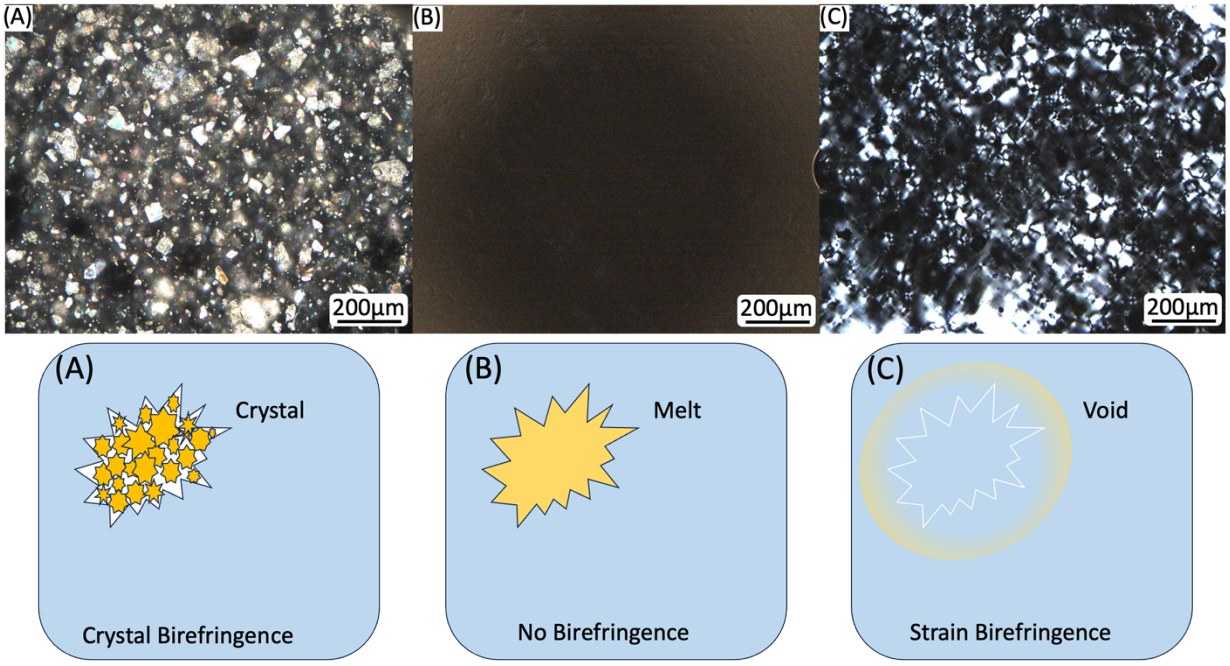

Figure 3. POM images of room temperature cured PT10 thermoset with birefringence from crystals present (A), after crystal melt at roughly 320 K (B), and after postcure annealing at 358 K for 20 mins with birefringence from polymer strain due to voids evident (C) with schematic of the crystal-to-void transition depicting how POM can be used to detect crystal inclusion or strain in the final polymer thermoset.

3.2 Isoconversional Analysis of Total Ion Thermographs

Prior to PSK analysis, the degradation kinetics of the thermoset was identified with isoconversional analysis of both thermogravimetric analysis (TGA) and EGA-MS. Mass loss profiles from TGA and corresponding conversion plots at heating rates of 5, 10, and 20 K/min are shown in Figure 4. The profiles of both thermosets look nearly identical with an initial mass loss starting around 450 K and the primary mass loss occurring above 600 K for both room temperature cured and post cure annealed conditions. It is important to note that the TGA profiles of PT at 5 K/min were inconsistent with the other TGA profiles displaying an additional mass loss at higher temperatures, resembling degradation under oxidative conditions. This is possibly due to a leak in

the instrument at the time of the measurments. Therefore the TGA data for the PT thermoset at 5 K/min was not used in the analysis for this work. While the International Confederation for Thermal Analysis and Calorimetry recommends using three different heating rates, the use of only two heating rates still yields viable kinetic information. [23] The calculated activation energies from this data follows the same trend as the PT [PC] sample, reaffirming that two heating rates are sufficient for calculating the kinetics.

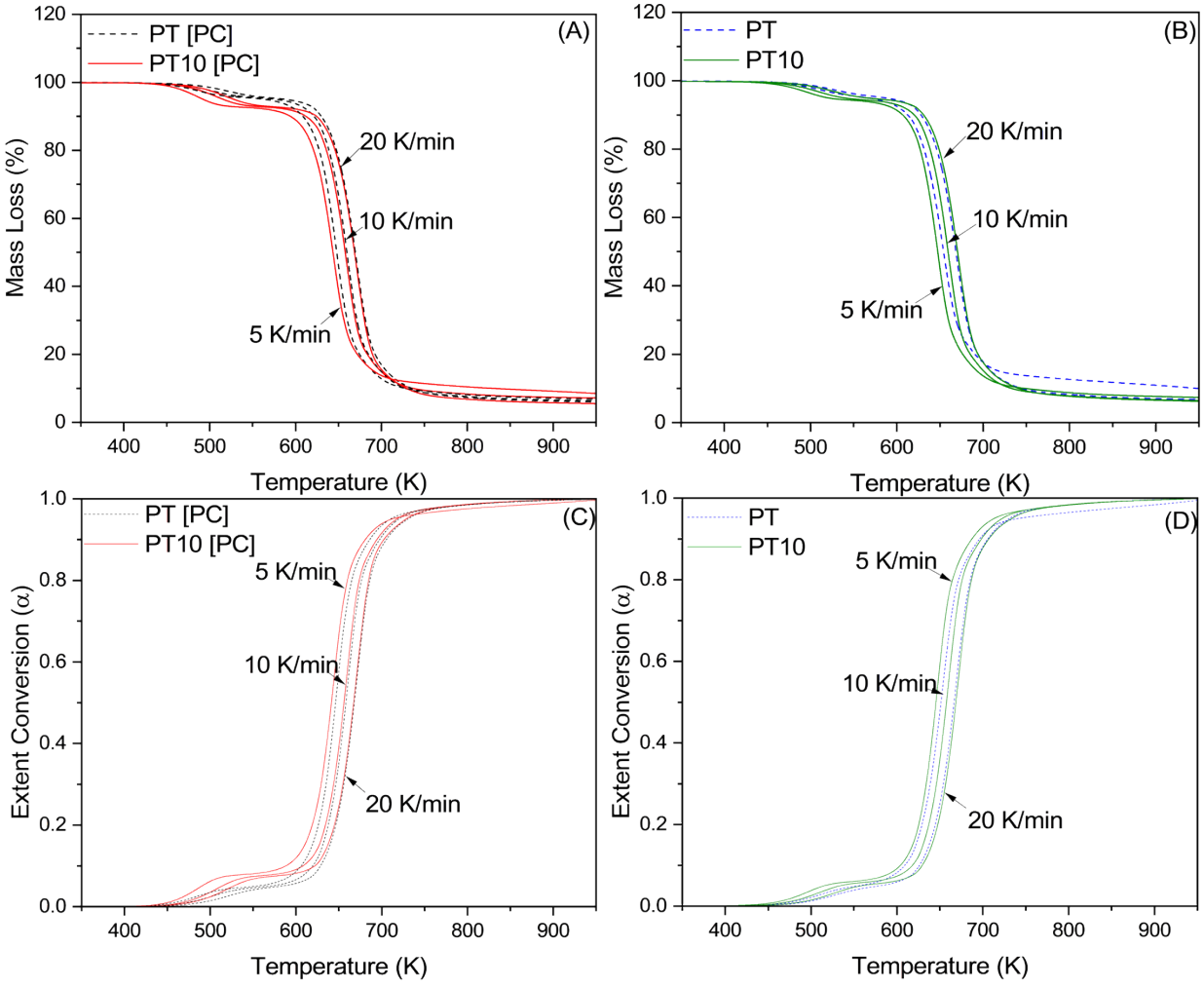

Figure 4. TGA of PT and PT10 thermosets post cured annealed (A) and cured at room temperature (B) and corresponding conversion plots showing nearly identical profiles and conversions for post cured annealed (C) and room temperature cured (D).

The averaged char yields for the TGA experiments were also evaluated in Figure 5. Because only two trials were performed, a quantitative comparison of the char yields is not possible. However, a qualitative comparison of the char yields reveal some trends. At the fastest heating rate of 20 K/min, the post-cure annealed samples appear to have less char yields than the room temperature cured thermosets, Figure 5A. At 10 K/min, this difference is further exaggerated between PT and PT [PC], Figure 5B, but the trend appears to be flipped for PT10 and PT10 [PC]. Finally, this flipped trend is further magnified at the slowest heating rate of 5 K/min for PT10 and PT10 [PC], Figure 5C. Unfortunatly, for the reason mentioned above, the TGA data for PT at 5 K/min was not obtained for the comparison of the PT data set. These results suggest there may be differences in the char formation between PT and PT10 thermosets which are further exaggerated by post-cure annealing.

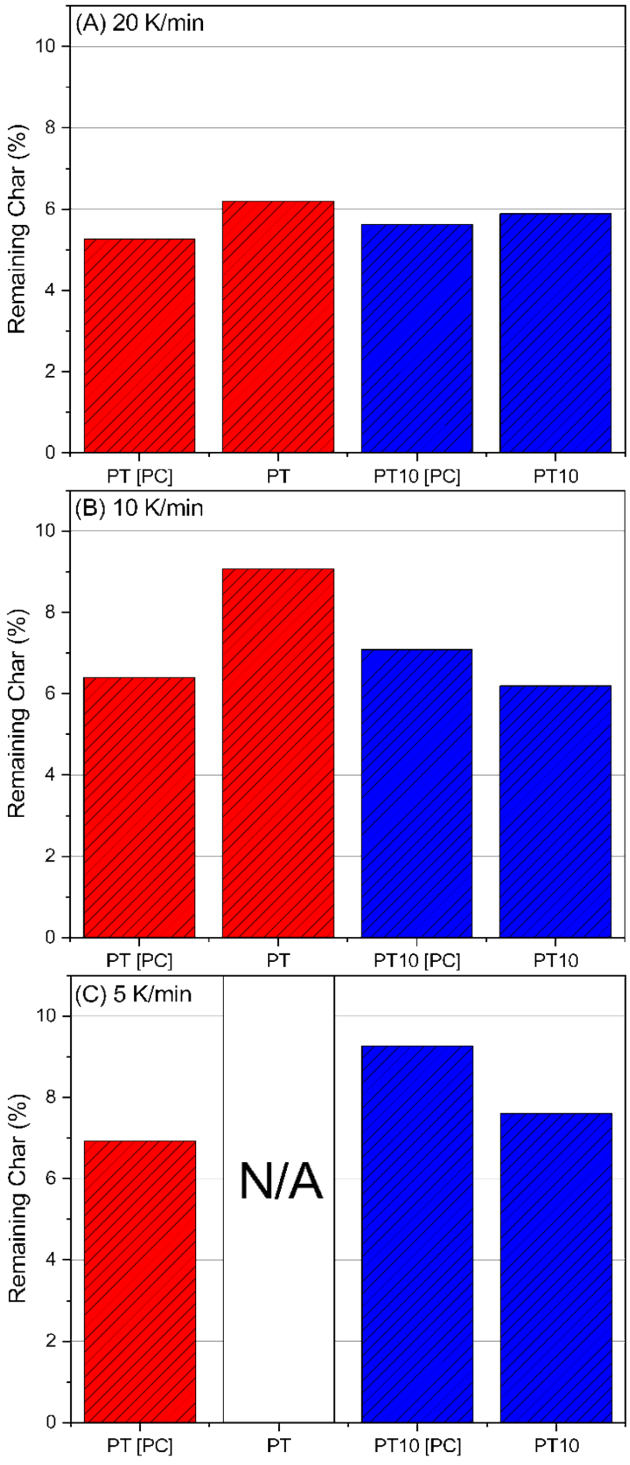

Figure 5. Average char yield for two trials of PT, PT10, PT [PC], and PT10 [PC] thermosets at 20 K/min (A), 10 K/min (B), and 5 K/min (C) heating rates.

Total ion thermographs (TITs) and corresponding conversion plots from EGA-MS experiments at heating rates of 5, 10, and 20 K/min are shown in Figure 6. These profiles show no significant difference in the peak temperatures or peak shapes for either thermoset before and after post-cure. Closer inspection of the profiles between 460 and 560 K (Figure 6A, B inset) reveals higher relative signal for the PT10 thermosets. This is consistent with the TGA results showing a larger mass loss in this region for PT10 and PT10 [PC] thermoset. Considering this temperature range has been associated with thermal desorption products from epoxy thermosets, the increase in relative signal for PT10 suggests more unreacted components remain in the PT10 thermosets compared to the PT thermosets after a post cure annealing procedure for 17 hrs at 358 K.[9] This can be explained by a higher concentration of unreacted monomers in the PT10 thermosets from the integrated crystals. However, as will be discussed later, not all of this signal for PT10 is attributed to thermal desorption products.

It is important to note that quartz wool is used in the EGA-MS experiments to prevent the sample from falling out of the Eco-cup during degradation. For the majority of EGA-MS experiments, the samples were prepared with quartz wool from a single batch. However, the results shown in Figure 6B/D and Figure 15 used quartz wool from a different batch which had some organic contaminants, Figures S1and S2. Fortunately, the signal from the contaminants is weak with respect to the TIT profiles, which can be observed in Figure 6B as the lower temperature peak around 450 K, so it is not suspected to significantly impact the final results.

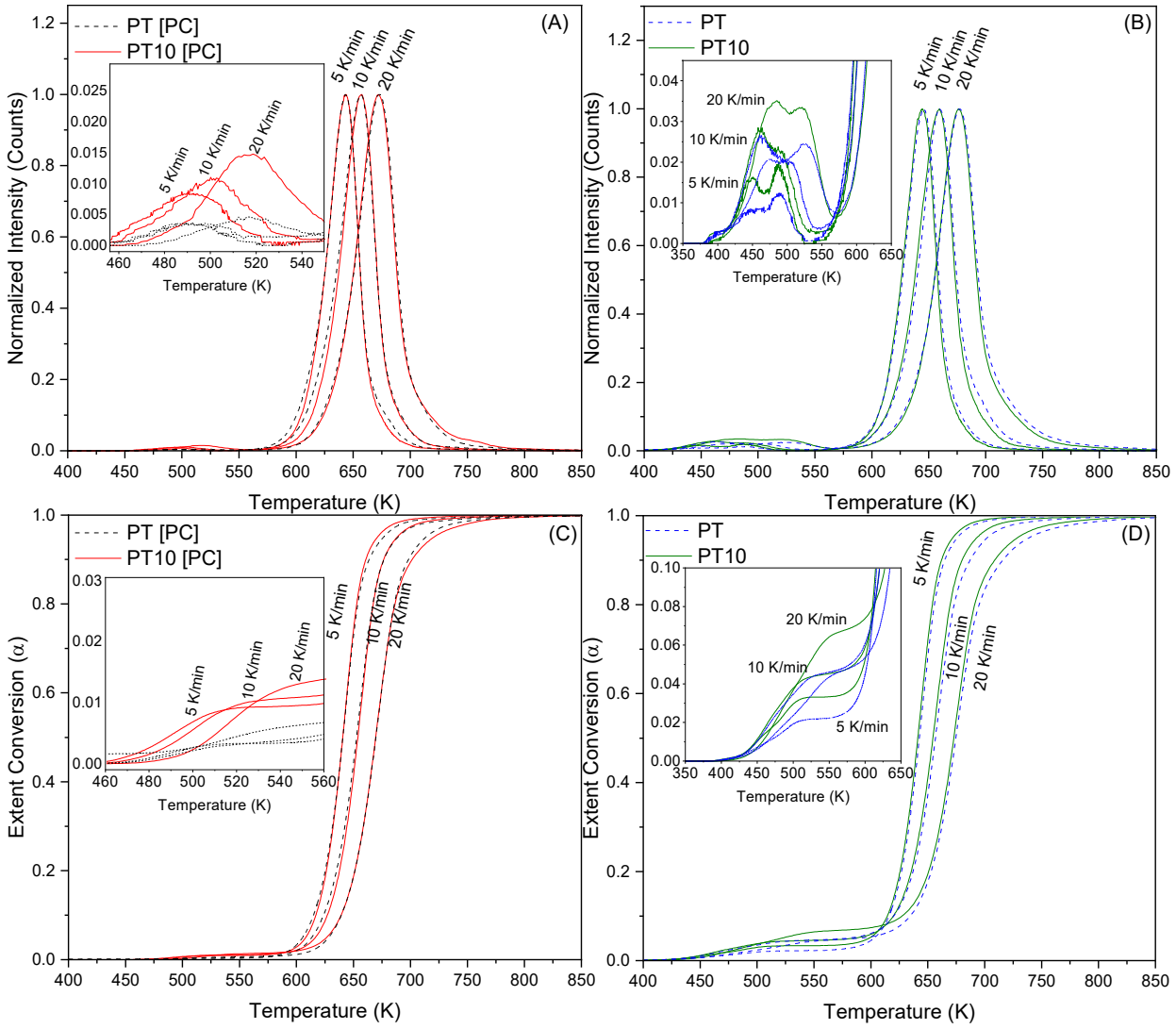

Figure 6. Total ion thermographs of PT [PC] and PT10 [PC] thermosets (A), PT and PT10 (B) and corresponding conversion plots, showing nearly identical profiles and conversions for post cured annealed (C) and room temperature cured (D). Inset graphs magnify the lower temperature region.

The calculated apparent E_a for the TGA and EGA-MS experiments are shown in Figure 7, with corresponding kinetic plots from EGA-MS and TGA data in Figures S3-S10. Overall, the E_a derived from EGA-MS are lower than that of TGA. This lower E_a is due to the fact that the sample

mass used in EGA-MS is significantly lower than in TGA, mitigating thermal effects from larger sample masses.[39] The trends in the apparent E_a for TGA appear consistant between PT and PT10 with and without post cure annealing, Figure 7AB, with an initial increase in E_a from 0.1-0.2 α and remaining unchanged until around 0.7 α where the E_a increases. Post-cure annealing appears to have opposite effects on the overall E_a with PT [PC] having higher apparent E_a than PT and PT10 [PC] having lower apparent E_a than PT10. This response corresponds to the trends observed in the char formation, suggesting a decrease in char formation corresponds to an overall increase in E_a and vice versa. The apparent E_a derived from the EGA-MS experiments shows a different trend than TGA, with apparent E_a starting at higher E_a and gradually decreasing. For EGA-MS experiment,s post-cure annealing has minimal impact on the apparent E_a with only minor changes observed, Figure 7CD, specifically, in EGA-MS analyses, an increase in E_a is seen at 0.7 α and above for PT thermoset, Figure 7C, while an increase in E_a for PT10 is seen at 0.1 α, Figure 7D. The large differences in the trend of apparent E_a between the TGA and EGA-MS results are a testament to the fact that EGA-MS is blind to char that forms, preventing evolution of the EGA-MS, while TGA captures all of the char formation in the degradation process. This reinforces the powerful and complementary nature of TGA and EGA-MS techniques for kinetic analysis and material degradation insights.

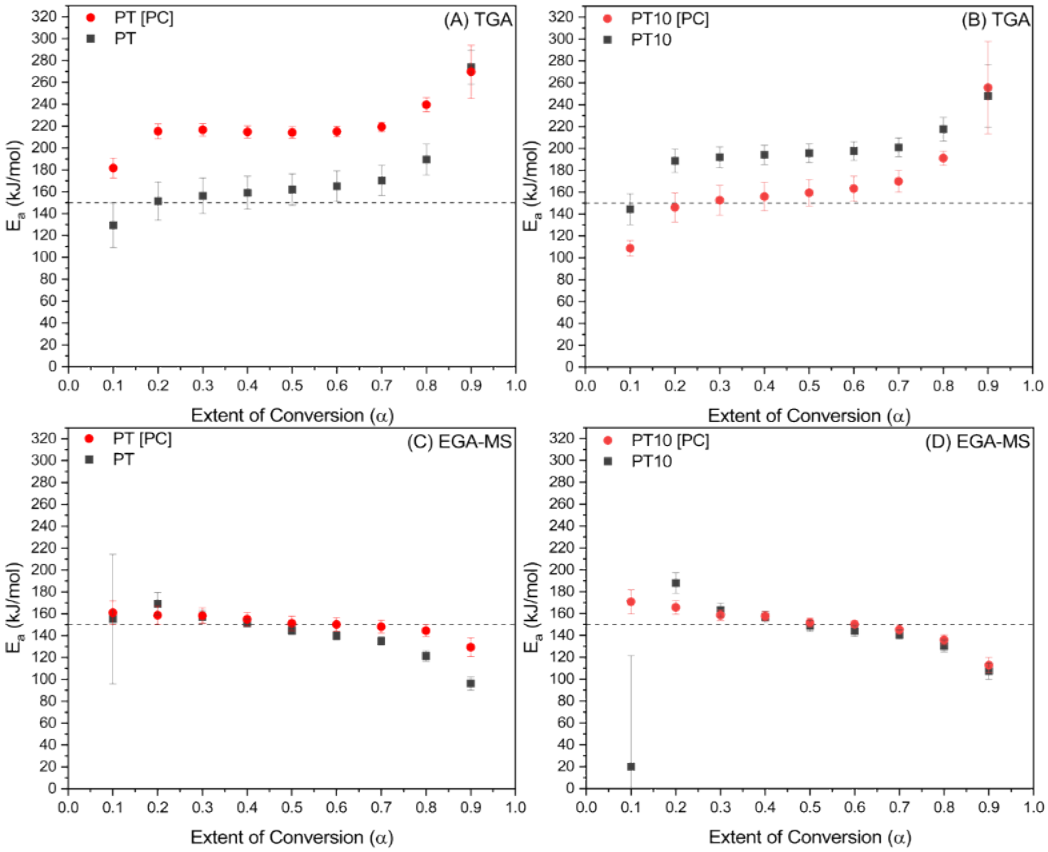

Figure 7. Apparent E_a values of PT (without crystal inclusion) and PT10 (with crystal inclusion) thermosets before and after post-cure annealing for 17 hrs at 358 K determined through TGA (A,B) and EGA-MS (C,D). The apparent difference in the apparent Ea values between the techniques attributed to the different sensitivity of each technique to char formation encountered during the conversion process.

3.3 Selection of Unique Product Ions

Ions *m/z* 66, 182, and 200 were previously identified as unique ions to phenol, xanthene, and bisphenol F monomer, respectively.[10] These three products were selected here because they are major degradation products of bisphenol F based epoxy thermosets. Bisphenol F monomer is produced from fragmentation at the two oxygen sites in the polymer structure, Figure 8. Further

fragmentation at the bridging carbon in the bisphenol F structure yields phenol.[40] Xanthene also forms from bisphenol F via a condensation reaction but is only possible with the o'o-bisphenol F isomer.[40] To confirm that the selected ions are still unique to the desired products, pyrolysis-gas chromatography – mass spectroscopy (PY-GC-MS) was performed. Ions *m/z* 66, 182, and 200 were extracted from the resulting total ion chromatograph, Figure 9. Extracted ion chromatographs of the selected ions confirm the majority of the ion signal comes from the desired products, as seen in preceding work.[10]

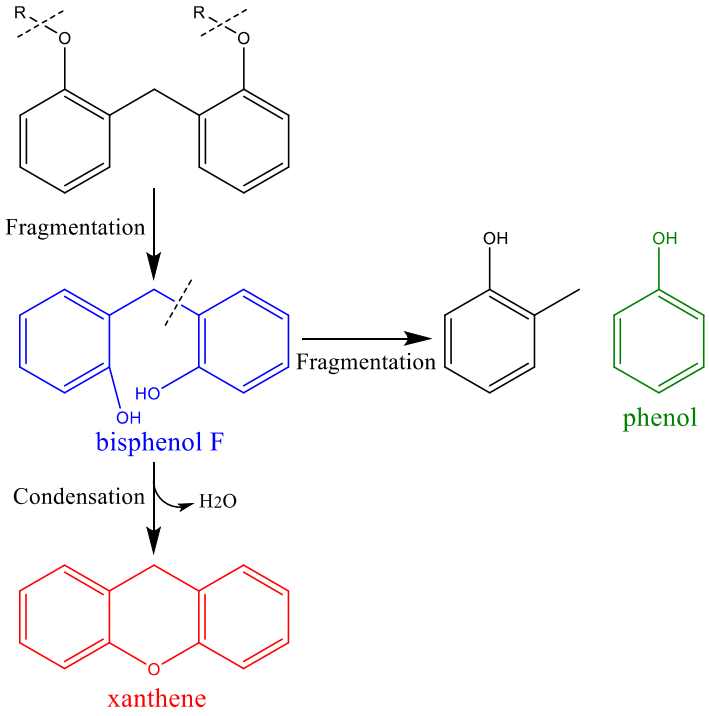

Figure 8. Formation mechanism of bisphenol F, xanthene, and phenol products from the polymer thermoset during thermal degradation.

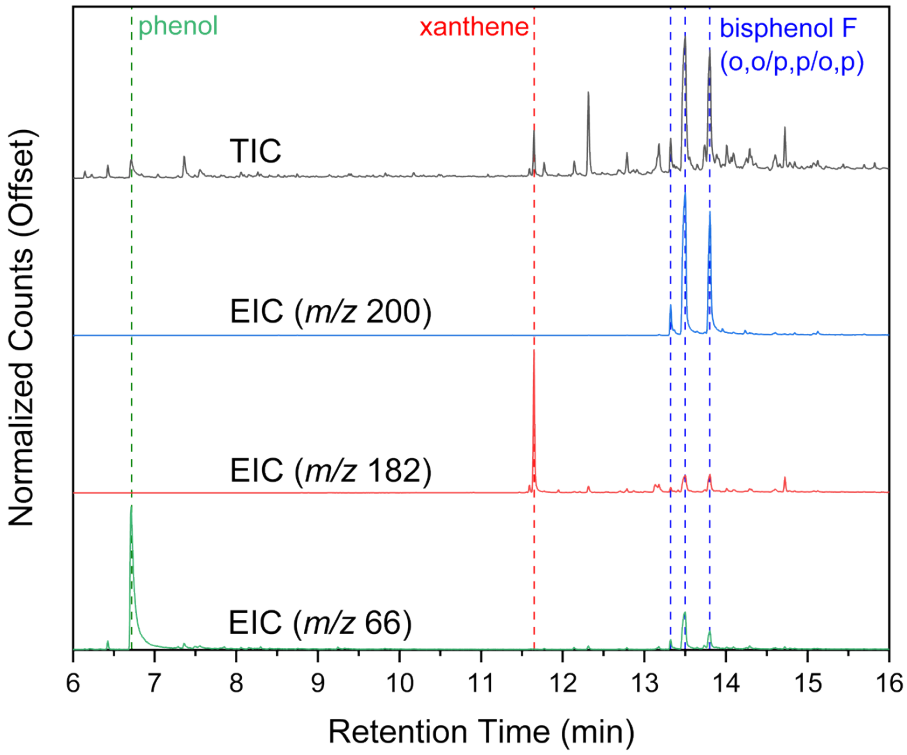

Figure 9. Total ion chromatograph (TIC) with extracted ion chromatographs (EICs) of ions *m/z* 200, 182, and 66 showing their uniqueness for their corresponding bisphenol F, xanthene, and phenol products.

3.4 Ion *m/z* 66 – Phenol

Extracted ion thermographs (EITs) of the phenol ion (*m/z* 66) for PT, PT10, PT [PC], and PT10 [PC] thermosets heated at rates of 5, 10, and 20 K/min are shown in Figure 10. Corresponding conversion and kinetic plots are shown in Figures S11 and S12. The thermal profiles of thermosets cured at room temperature overlap closely, as shown in the EITs in Figure 10B. Two thermal zones emerge for both room temperature and post-cure annealed thermosets: a sharp peak constituting the bulk of the signal from 550 to 750 K, and a tailing peak from 750 to 900 K. The sharp peak is associated with thermoset degradation, and the tailing peak is suspected to result from degradation of char formed after the initial degradation of the polymer network.

The peak evolution temperature is shifted to slightly lower values for crystal included PT10 versus PT. The E_a values of the phenol product (Figure 10B inset) show that pathways for degradation in both PT and PT10 thermosets follow similar trends from 0.4 to 0.9 α, with PT10 on average having lower E_a. More significant differences are observed after post cure annealing (Figure 10A). PT [PC] shows a significantly higher E_a than PT10 [PC] from 0.3 to 0.8 α, as shown in Figure 10A. This increase in relative E_a for PT [PC] is accompanied by minor changes in the EITs, which show an apparent decrease in the relative intensity of the tail signal around 750–900 K. This decrease can be interpreted as either less char formation for PT [PC] or increased char formation for PT10 [PC]. Results shown in Figure 5 comparing apparent E_a extracted from TGA and EGA-MS suggest both statements are correct.

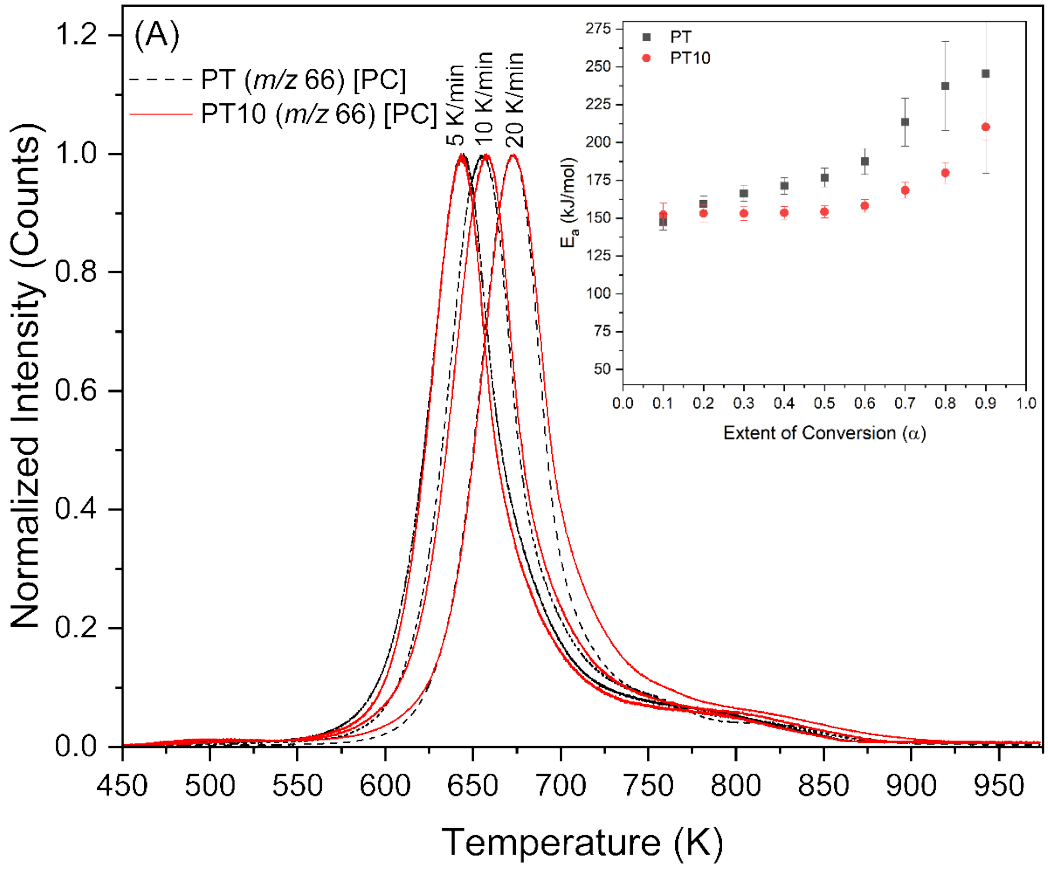

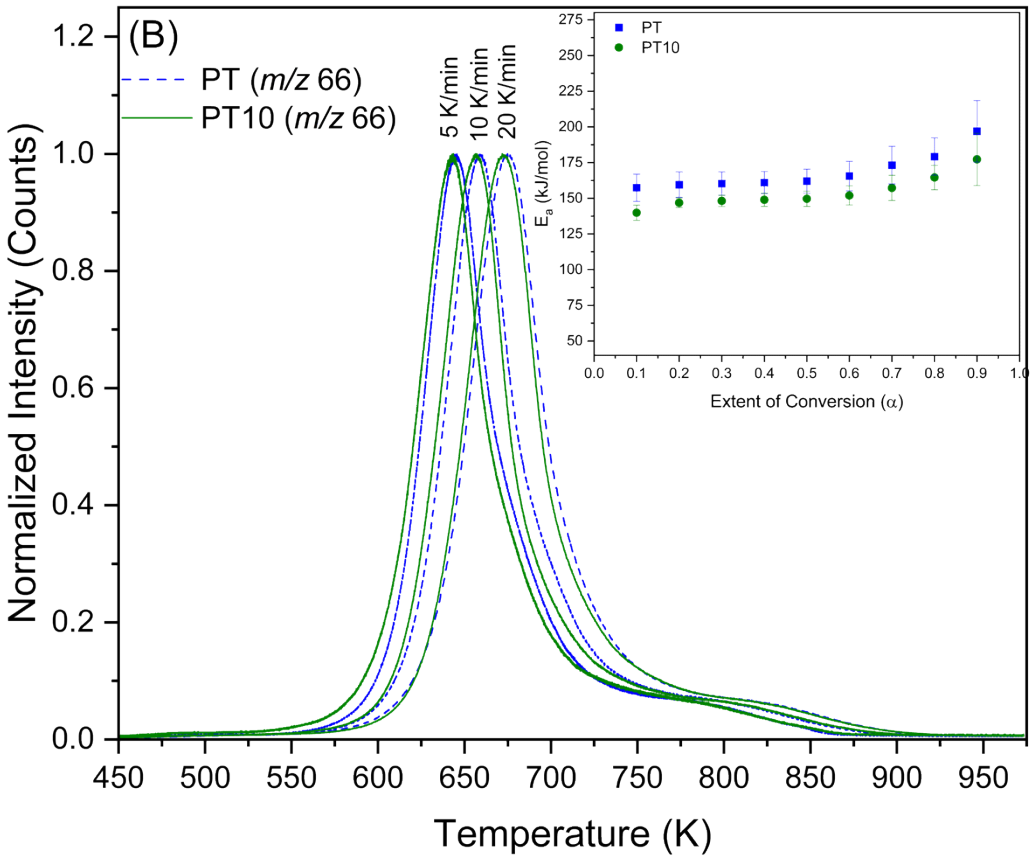

Figure 10. EITs of the phenol ion (*m/z* 66) at 5, 10, and 20 K/min heating rates for PT [PC] and PT10 [PC] thermosets (A) , PT and PT10 thermosets (B). Both (A) and (B) include inset plots of apparent E_a with respect to extent of conversion calculated from PY-GC-MS extracted ion data.

3.3 Ion *m/z* 182 – Xanthene

EITs and E_a values for the product xanthene ion (*m/z* 182) are shown in Figure 11; corresponding conversion and kinetic plots are shown in Figures S13 and S14. The EITs of xanthene (*m/z* 182) for PT and PT10, shown in Figure 11B, have a minor peak from 450 to 575 K and a major peak from 550 to 800 K. The major peak is within the range designated as degradation of the polymer, and the PT and PT10 peaks overlap for both curing conditions. The apparent E_a values for PT and PT10 thermosets are statistically lower for PT10 than PT for 0.1–0.9 α, as shown in Figure 11B.

On the other hand, notable differences in the apparent E_a values of PT [PC] and PT10 [PC] thermosets are observed only up to 0.3 α, as shown in Figure 11A.

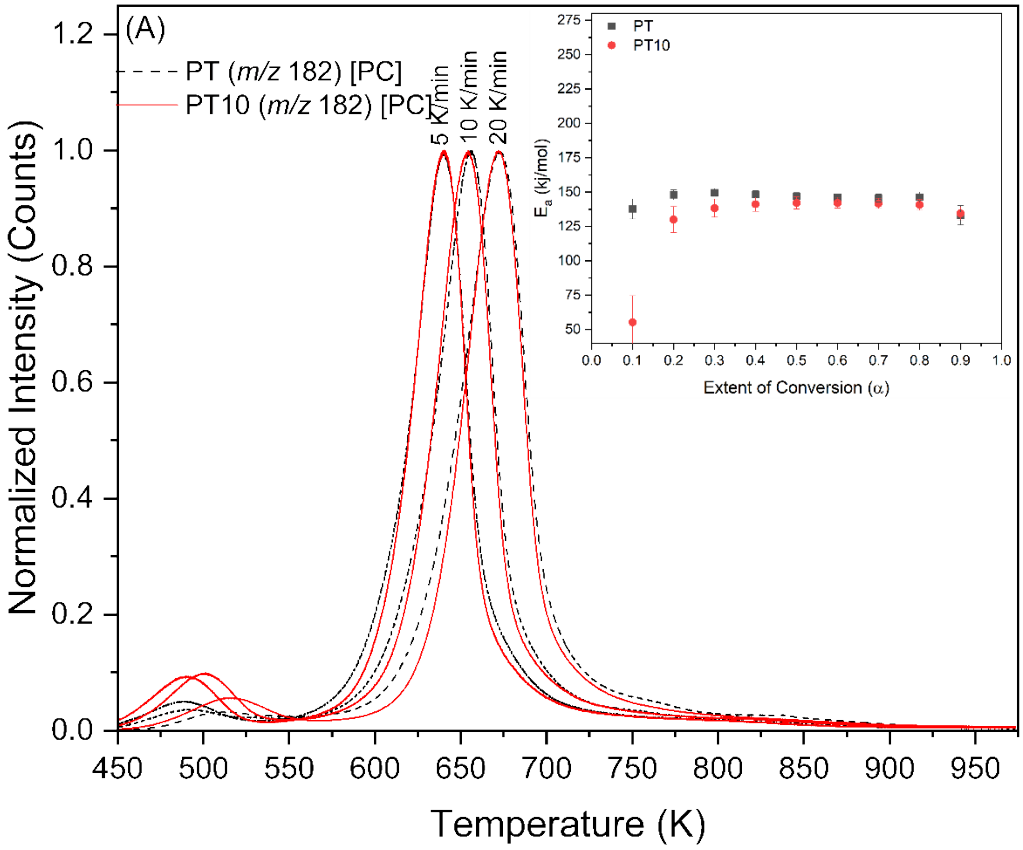

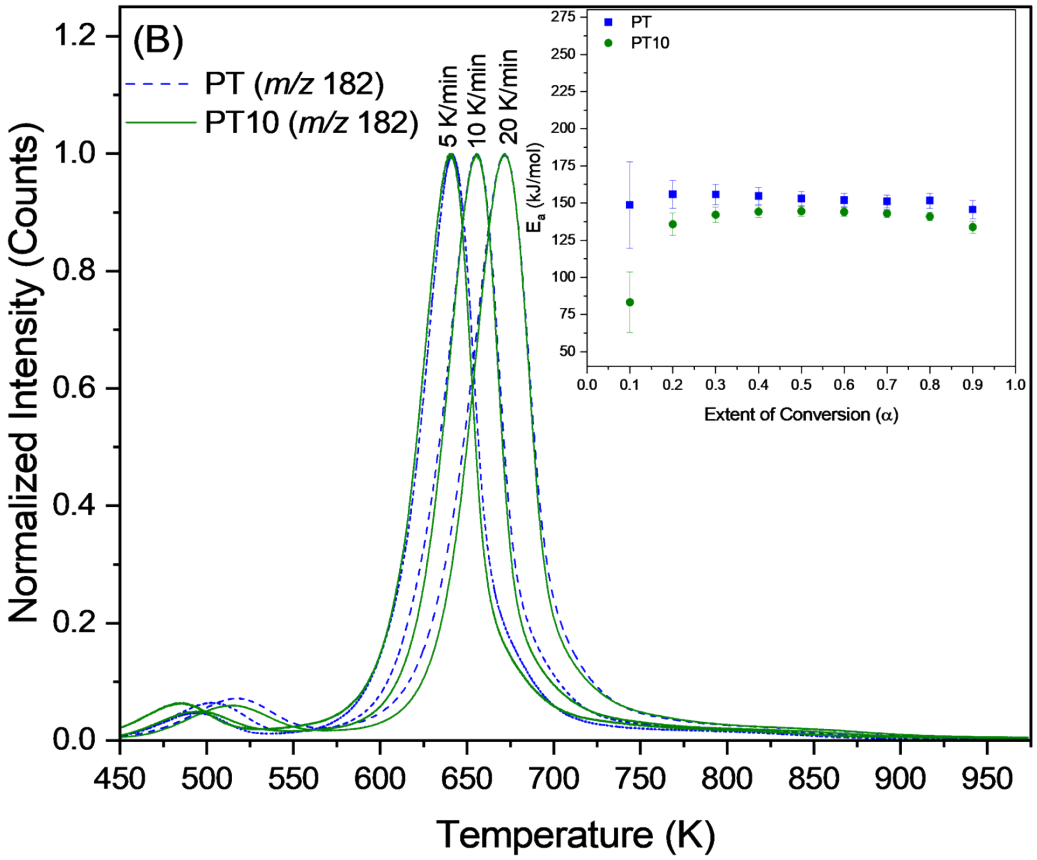

Figure 11. EITs of the xanthene ion (*m/z* 182) at 5, 10, and 20 K/min heating rates for PT [PC] and PT10 [PC] thermosets (A) , PT and PT10 thermoset (B). Both (A) and (B) include inset plots of apparent E_a with respect to extent of conversion calculated from PY-GC-MS extracted ion data.

Lower temperature peaks in total ion thermographs have been associated with thermal desorption.[9] However, xanthene is not a product present in the uncured resin or hardener.[38] Further investigation was performed to identify the source of this low temperature peak. Closer inspection of the minor peak before and after post cure annealing are shown in Figure 12. After post cure annealing, the relative intensity of the minor peak decreases for the PT [PC] thermoset at all three heating rates. This is consistent for each trial performed, shown in Figure 13. Conversely, the relative intensity of the minor peak increases for the PT10 [PC] thermoset at all three heating rates.

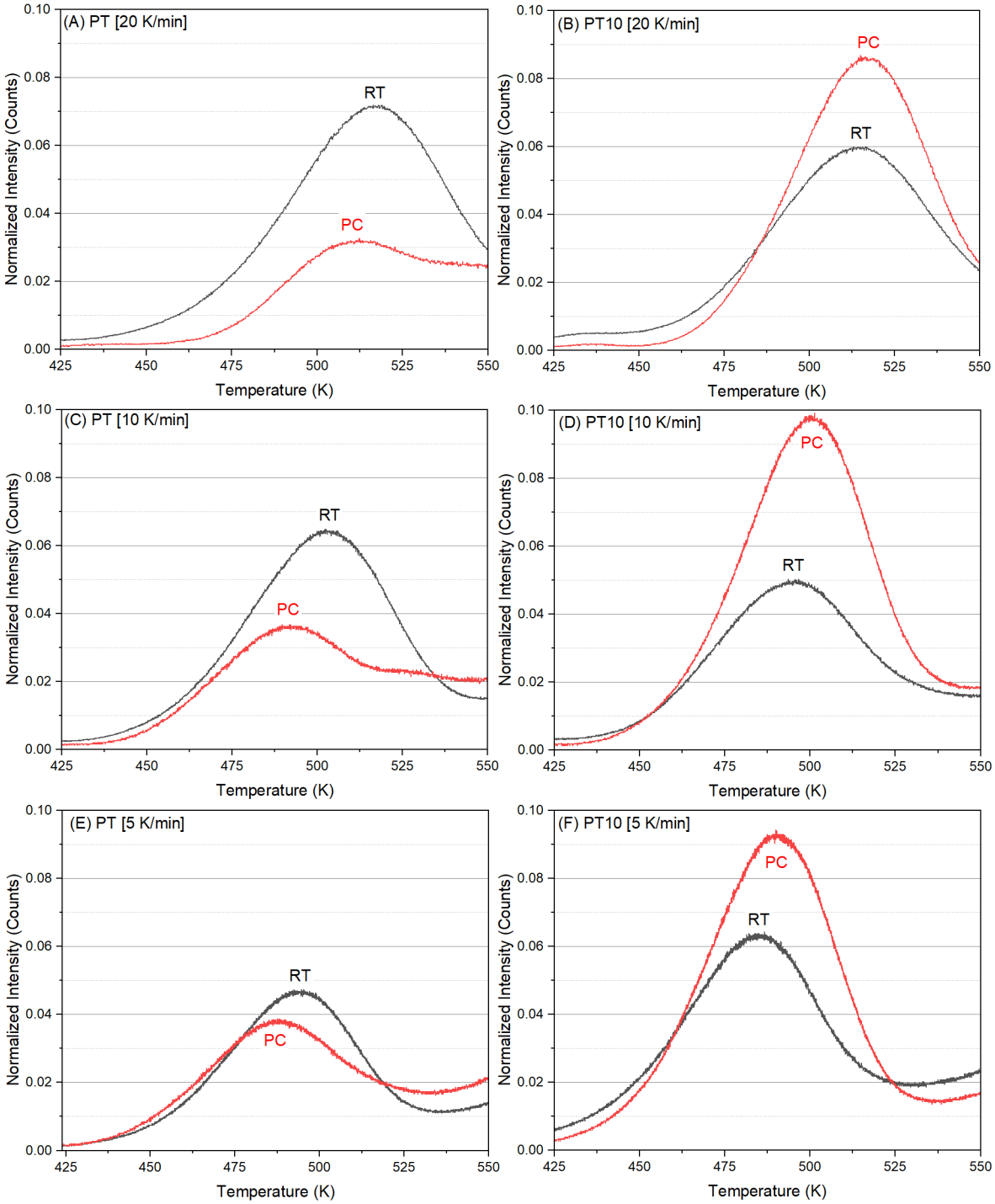

Figure 12. EITs of the minor peak proposed to arise from the xanthene ion (*m/z* 182) for PT at (E) 5, (C) 10, and (A) 20 K/min heating rates and PT10 at (F) 5, (D) 10, and (B) 20 K/min heating rates for thermosets post cure annealed (PC) at 358 K for 17 h and cured at room temperature (RT).

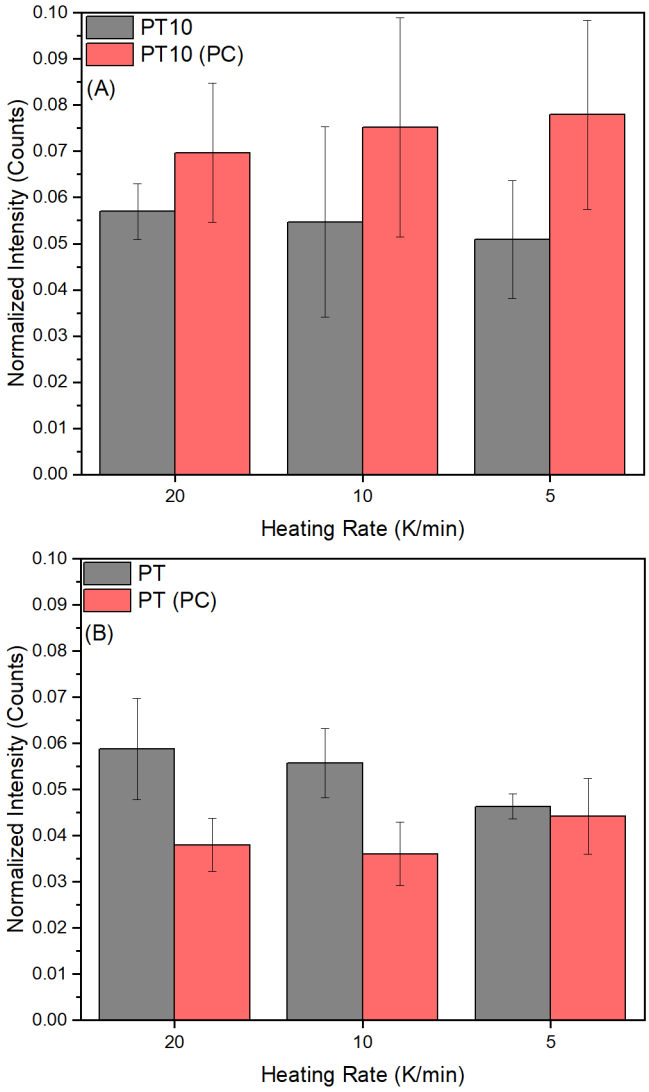

Figure 13. Normalized average intensity of the minor peak proposed to arise from xanthene ion (*m/z* 182) for PT, PT10, PT [PC], and PT10 [PC]. The average peak intensity associated with the xanthene ion increased for PT10 [PC] (A) and decreased for PT [PC] (B).

The presence of partially bound monomers and their subsequent cleavage and removal during heating explains the existence of the minor peak associated to xanthene and the difference in response between PT [PC] and PT10 [PC] thermosets. Thermoset curing causes the molecular weight and cross-linking density of the forming polymer to increase. At a certain time and temperature, the polymer hardening prevents further migration of reactive components, resulting

in incomplete cure that leaves partially bound or unbound epoxy monomers. A post cure annealing procedure allows for greater mobility of the unreacted components in the polymer network. This mobility permits further reaction with nearby unreacted components, increasing the cross-linking density and decreasing the concentration of partially bound or unreacted monomer components. This process explains the observed decrease in the minor peak intensity for the PT [PC] thermoset, Figure 14.

In the case of the PT10 thermosets, most of the uncured monomers are unbound and condensed in a crystallized form. During post cure annealing, the epoxy crystals melt, and the released unbound monomers migrate into the polymer network, Figure 3C. In principle, these monomers would bind at available reactive sites. However, because the thermoset network is formed *before* the PT10 post cure annealing, we propose that these monomers bind in unfavorable positions in the highly branched polymer network, preventing complete binding into the network. A diagram of this proposed process is shown in Figure 14. This increase of partially bound monomers, caused by the melting of epoxy crystals, would explain the increase in the observed minor peak intensity (Fig. 11-13) for *m/z* 182 ion.

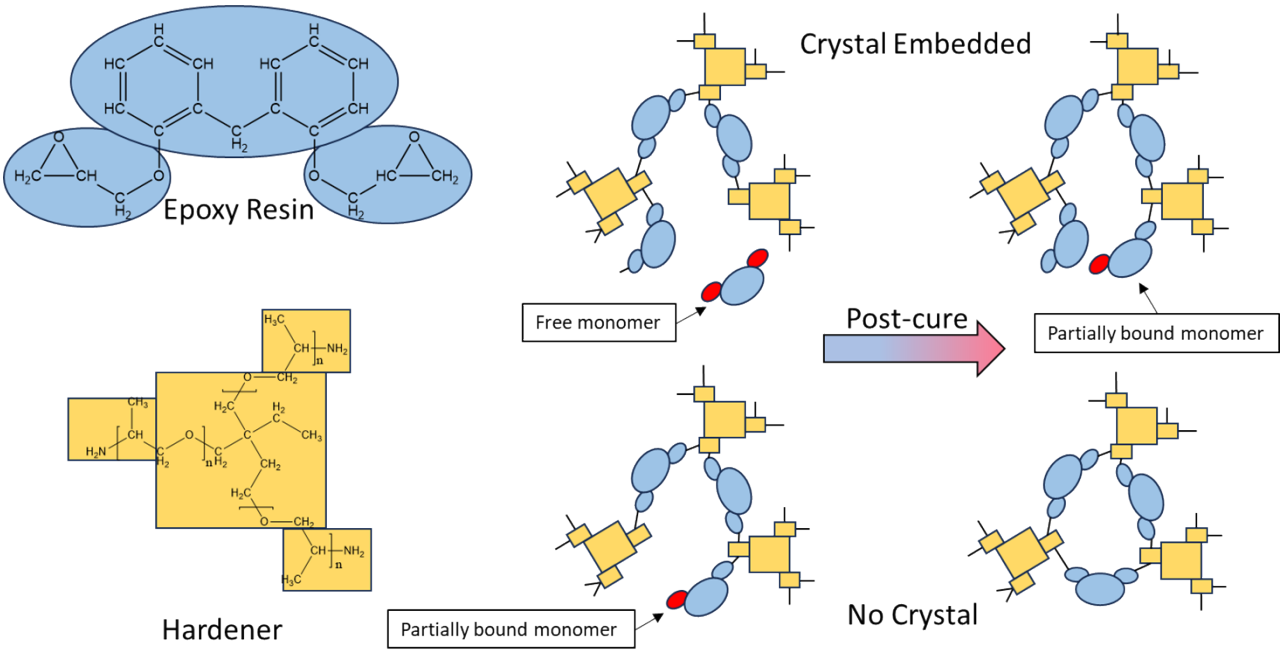

Figure 14. Diagram of proposed partial bonding of free monomer released from epoxy crystal melting showing how unfavorable positioning of a bound monomer prevents complete bonding into polymer network.

The question remains as to whether the *m/z* 182 ion at lower temperatures is still due to xanthene or some unknown product from partially bound monomers. Thermal desorption (TD)-GC-MS was performed on the samples to identify specific product(s) that are produced in this temperature region. The TIC of the TD-GC-MS analysis for PT [PC], PT10 [PC], and the quartz wool are shown in Figure 15A. A significant amount of contamination is observed from this batch of quartz wool, explained earlier (section 3.2). But, both PT [PC] and PT10 [PC] have an additional peak at 14.8 min that is not present in the quartz wool control. This product does not match the retention time or mass spectra of xanthene, Figure 16. The major ions identified from the novel products mass spectra are *m/z* 256 and *m/z* 181, and the novel product has a significant contribution from *m/z* 182 confirming this product is the source of the lower temperature peak and not xanthene.

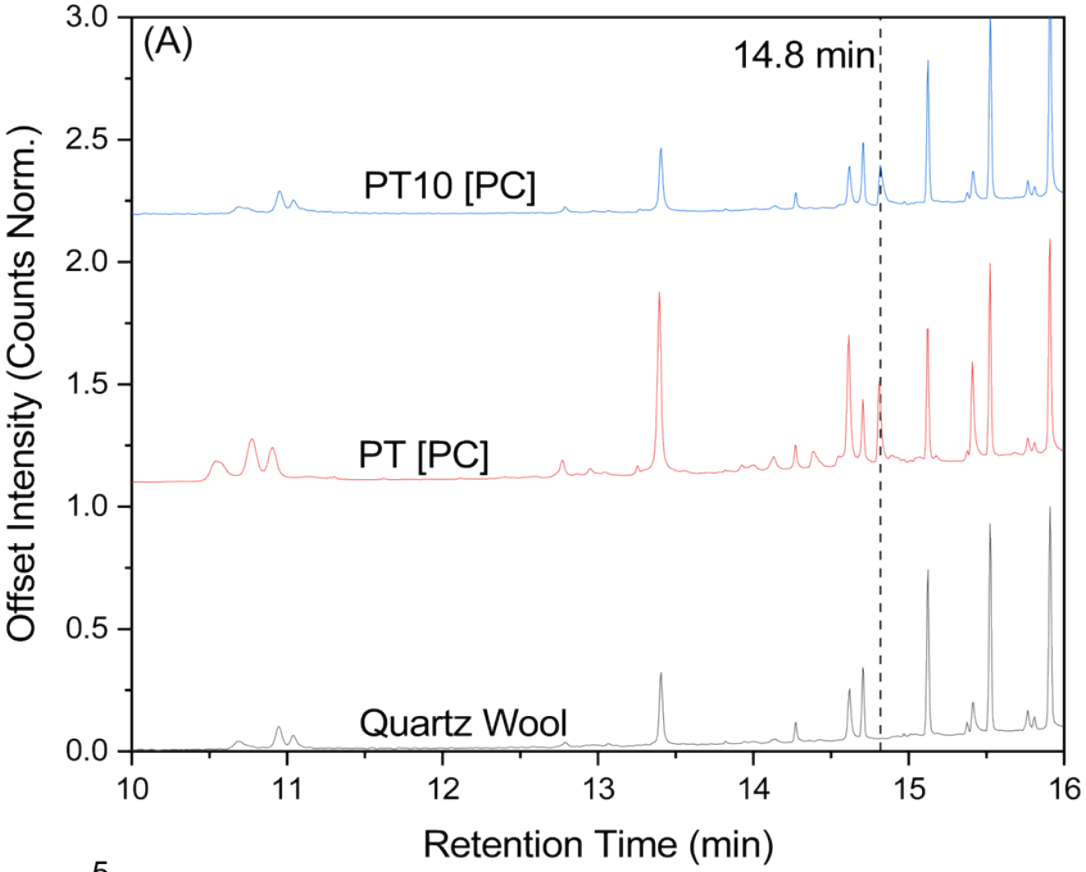
(A)
14.8 min
PT10 [PC]
PT [PC]
Quartz Wool
Offset Intensity (Counts Norm.)
Retention Time (min)
3.0
2.5
2.0
1.5
1.0
0.5
0.0
10
11
12
13
14
15
16

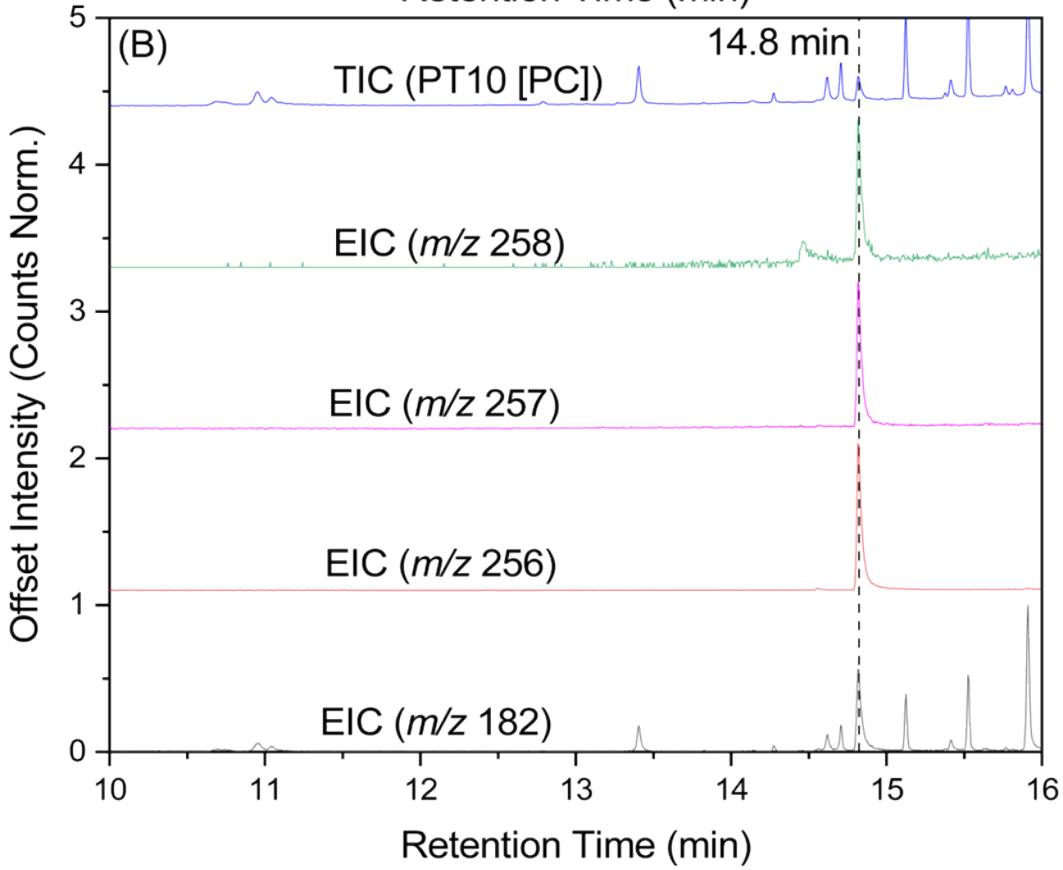
(B)
14.8 min
TIC (PT10 [PC])
EIC (m/z 258)
EIC (m/z 257)
EIC (m/z 256)
EIC (m/z 182)
Offset Intensity (Counts Norm.)
Retention Time (min)
5
4
3
2
1
0
10
11
12
13
14
15
16

Figure 15. Total ion chromatographs of Quartz wool, PT [PC], and PT10 [PC] (A) and EIC of ions *m/z* 258, 257, 256, and 182 for TIC of PT10 [PC] (B).

Considering this product is thought to come from a partially bound monomer, its structure is postulated to be a bisphenol F monomer with an epoxy functional group, shown in Figure 16. Using the predict mass spectra feature in ChemDraw (version 18.2.0.48), a predicted ratio of 100.0%, 17.3%, and 1.4% for *m/z* 256, *m/z* 257, and *m/z* 258, respectively, was obtained. The corresponding ratio determined experimentally was 100%, 18.3%, and 1.7%, close to the predicted values. To further support the identification of this novel product, density functional theory (DFT) calculations were performed to understand the bond energetics. Specifically, DFT sought to confirm whether the ether bond (1) connected to the polymer matrix is lower or equal in energy to the ether bond (2) connected to the free epoxy functional group, Figure 17. The physical insight from the calculation is that a significantly lower calculated bond energy for bond 2 would result in cleavage of the epoxy functional group prior to the monomer coming from the matrix, which would make the proposed structure unlikely.

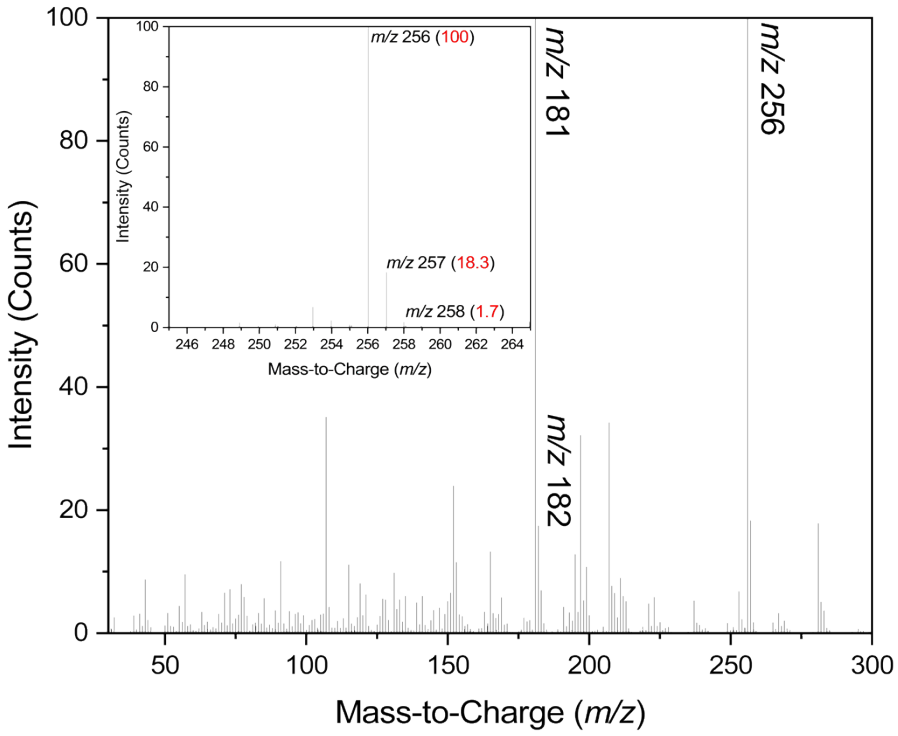

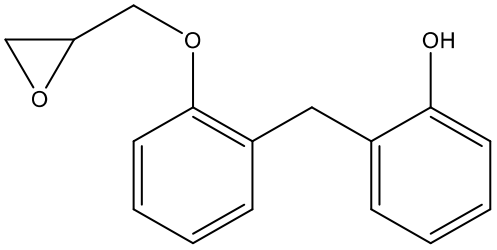

m/z: 256.11 (100.0%), 257.11 (17.3%), 258.12 (1.4%)

Figure 16. Mass spectra and predicted structure of the unknown product at 14.8 mins, hypothesized as a bisphenol F monomer with an epoxy functional group. The predicted mass spectra from ChemDraw is in good agreement with the experimental data (indicated in parentheses).

The amine-terminated bisphenol F epoxy monomer modeled with DFT includes two different ether substituents, differing in their neighboring terminal functional groups. One side is epoxy terminated while the other is amine terminated with a branching alcohol which represents

the functional group that binds the monomer to the polymer network, Figure 17. The bond energies were calculated to be 378 and 387 kJ/mol, respectively, in good agreement with the available literature values for ether C-O bonds.[41] Thus, the energy of the amine-neighboring ether C-O bond is slightly stronger than the epoxy-neighboring ether C-O bond, though this difference (8.6 kJ/mol) is fairly small. This suggests that both bond 1 and bond 2 are equally likely to break when subjected to the same thermal conditions, indicating the feasibility of the proposed structure in Figure 16.

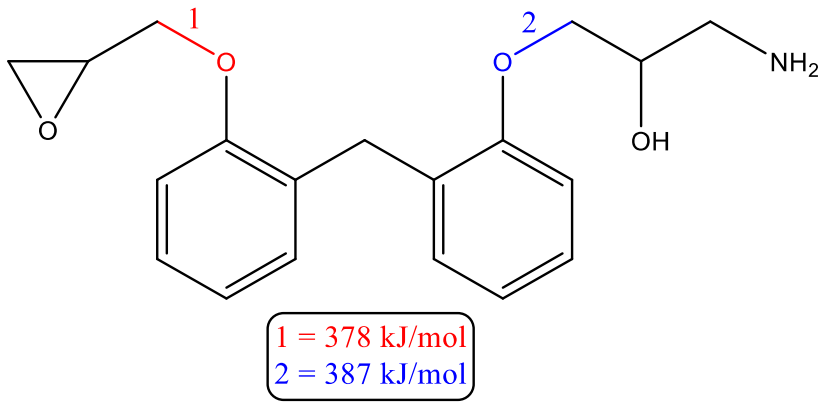

Figure 17. Hypothetical structure used in DFT model to determine the bond energy of the ether to epoxy functional group and ether to amine terminated alcohol functional group representing the functional group potentially anchoring the partially bound monomer to the polymer network. The bond energies calculated from DFT show that the bond energies are close and equally likely to break when subjected to thermal degradation conditions, thus rendering the proposed model of the novel low temperature product as an amine-terminated bisphenol F monomer plausible.

3.4 Ion *m/z* 200 – Bisphenol F

EITs of the bisphenol F monomer (*m/z* 200) are shown in Figure 18; corresponding conversion extent and kinetic plots are shown in Figures S15 and S16. Unlike the case of phenol and xanthene,

the EITs for the bisphenol F isomer ions have a single peak from 550 to 750 K, which corresponds to degradation of the polymer thermoset. There are minimal differences between the thermographs for the two curing conditions. The apparent E_a plot in Figure 18B shows that before post cure annealing, E_a is lower for PT10 at 0.1 α, whereas the E_a values for PT and PT10 are statistically identical at conversion extents between 0.2 and 0.9 α. After post cure annealing, the PT10 [PC] thermoset has a significantly lower E_a at a conversion extent of 0.9 α. This response indicates that before post cure annealing, the kinetics of the bisphenol F product pathway at the early stages of degradation are significantly different for the crystal-integrated thermoset and the crystal-free thermoset. After post cure annealing, the kinetics are identical in the early stages for the crystal-integrated and crystal-free thermosets, but differences in the kinetics are observed in the final stages of degradation at high conversion extents. These trends in bisphenol F product kinetics correlate with xanthene and phenol and suggest that the presence of crystal in the thermoset has the greatest influence on thermoset degradation at the early stages of degradation.

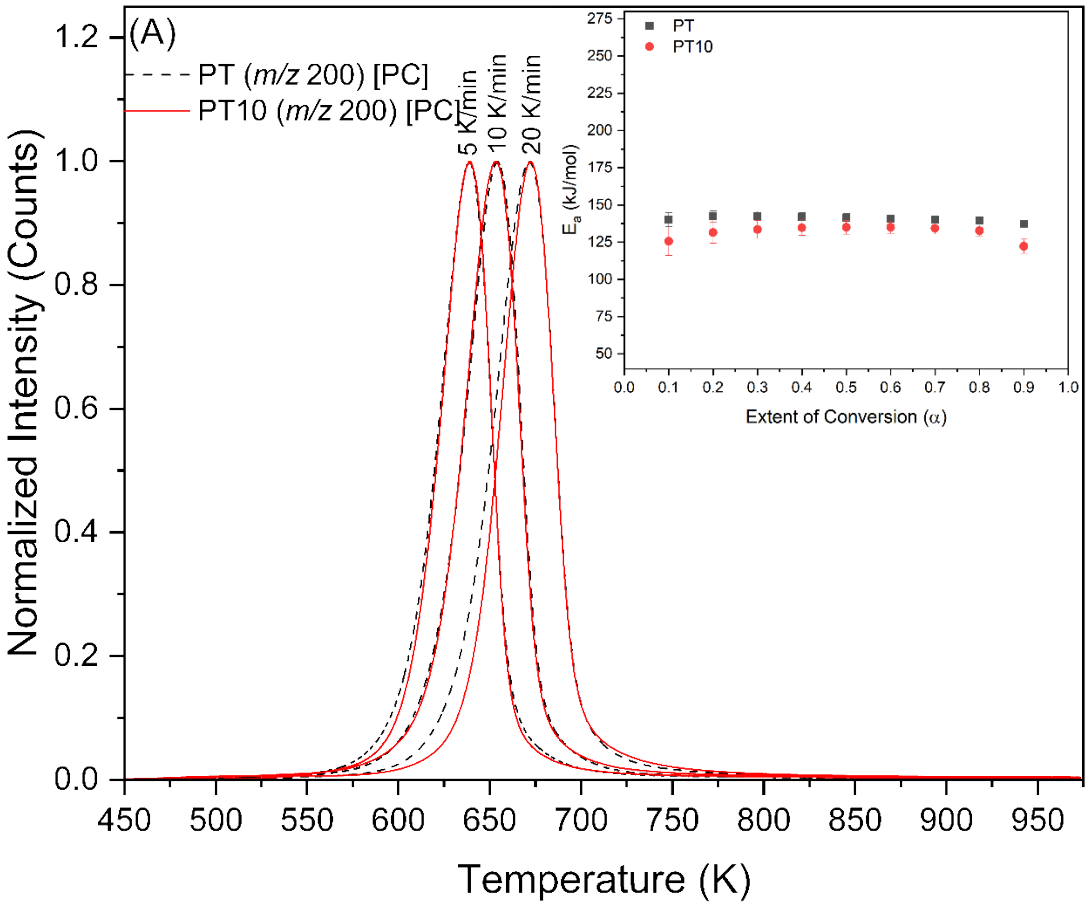
(A)
PT (m/z 200) [PC]
PT10 (m/z 200) [PC]
5 K/min
10 K/min
20 K/min
Normalized Intensity (Counts)
Temperature (K)
PT
PT10
Ea (kJ/mol)
Extent of Conversion (α)

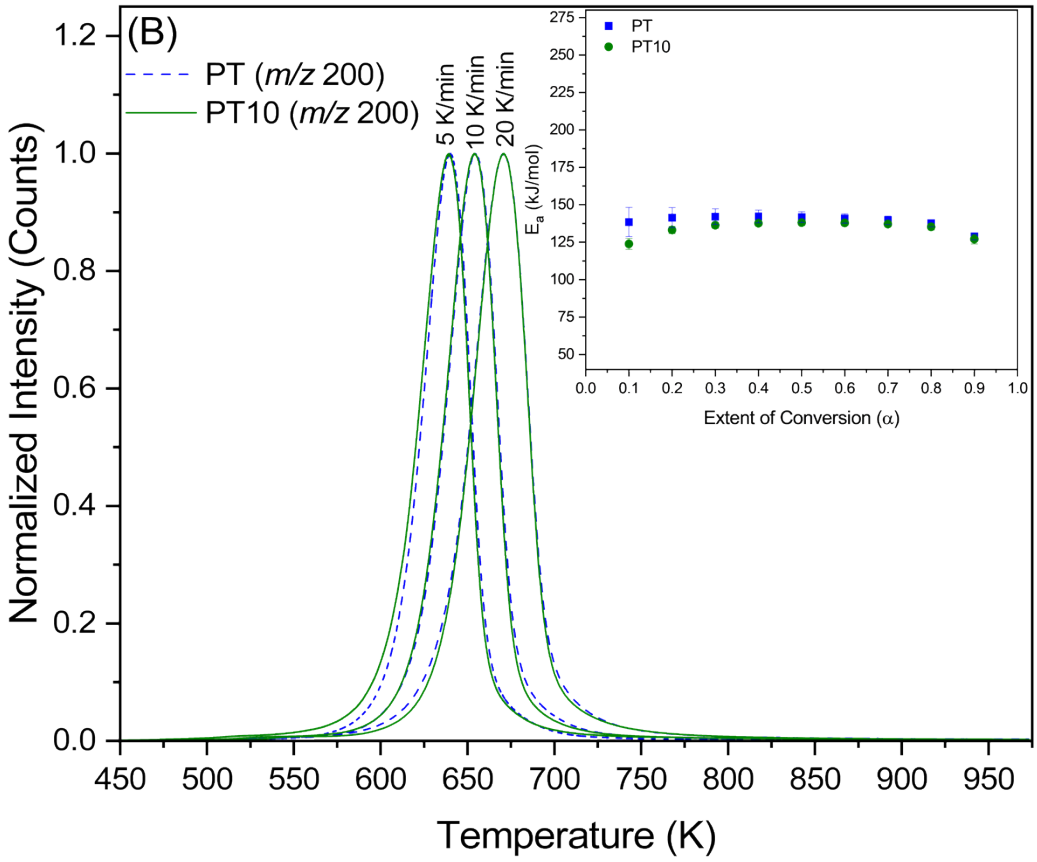

Figure 18. EITs of the bisphenol F monomer ion (*m/z* 200) at 5, 10, and 20 K/min heating rates for the PT [PC] and PT10 [PC] thermosets (A), PT and PT10 thermosets (B). Both (A) and (B) include inset plots of apparent E_a with respect to extent of conversion.

3.5 Impact of Post-Cure on PSK

Apparent E_a of all three ions evaluated for PT and PT10 before and after post cure annealing were compared to better understand the impact of crystal integration on degradation kinetics, Figure 19. PT and PT10 thermosets showed all three ions followed the same trend from 0.1 – 0.5 conversion with exception to 0.1 for PT10. Above 0.5 conversion, the E_a for ions contributing to phenol continue to increase. Post cure annealing does not alter these trends but does exaggerate the deviation of *m/z* 66 from this trend, especially in PT with a gradual increase in E_a starting at 0.2 conversion. These observation are explained by the expanded pyrolysis mechanism

shown in Figure 20. The formation mechanism for xanthene and phenol depend on the formation of bisphenol F monomer with further fragmentation at the bridging carbon causing phenol formation or, in the case of the o,o-bisphenol F isomer, condensation to form xanthene. These mechanisms explain the shared trend in the in E_a for most of the data up to 0.5 conversion, as well as the order in their E_a. Ion *m/z* 200 has the lowest energy because it is the first step, followed by *m/z* 182 which requires minimal energy for a condensation step to form xanthene. Finally, *m/z* 66 has the highest energy because of the additional fragmentation step. The deviation of *m/z* 66 to higher E_a before and after post cure annealing suggests the phenol product is coming from a different mechanism that does not have bisphenol F formation as a precursor step. It is proposed that the source of phenol from these later conversions are due to char formation and subsequent pyrolysis resulting in continuingly higher thermally stable material over the course of degradation, explaining the increasing E_a.

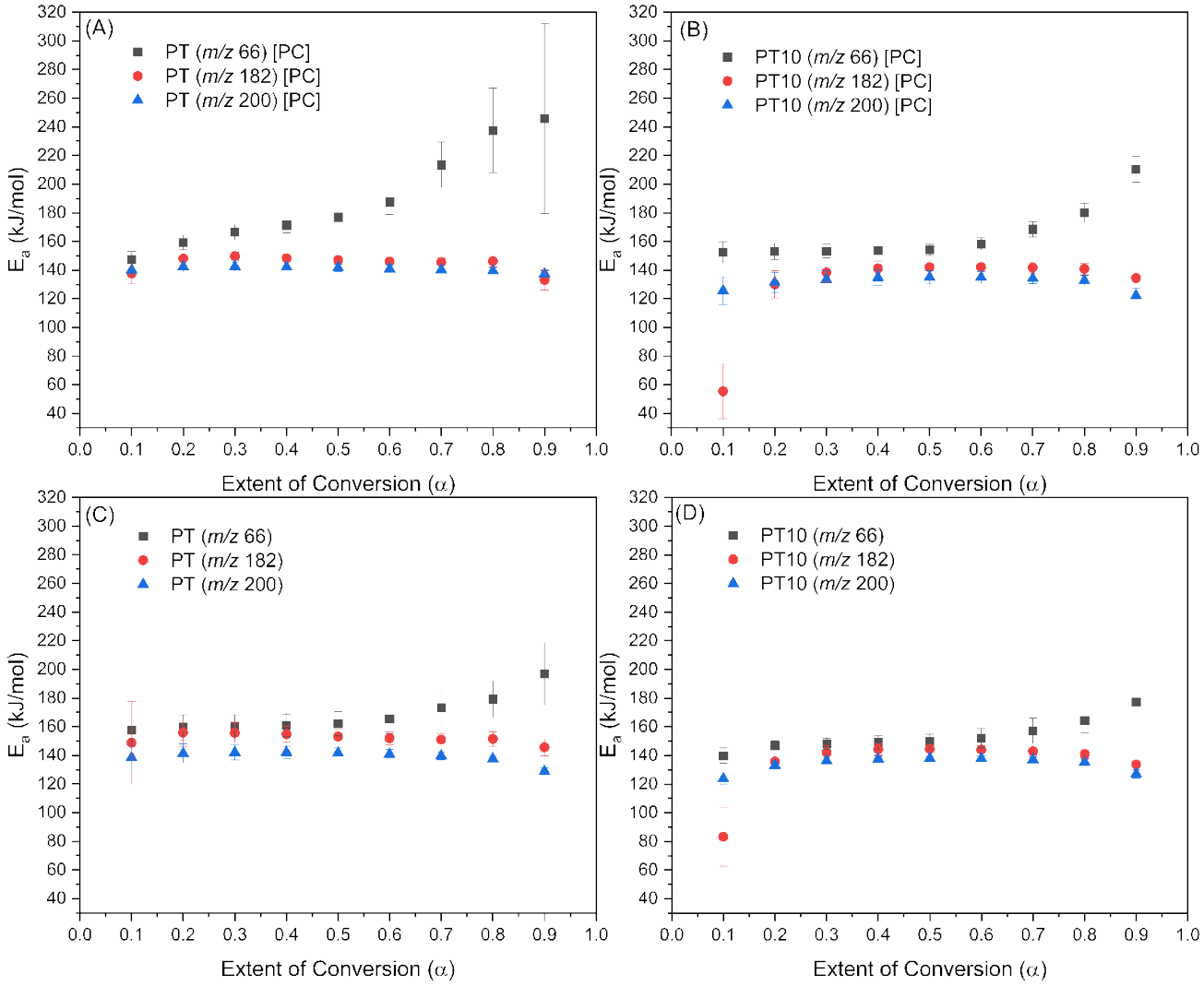

Figure 19. Apparent E_a of *m/z* 66, 182, and 200 for PT and PT10 before and after post-cure annealing.

The lower E_a of *m/z* 182 at 0.1 conversion for the PT10 and PT10 [PC] thermosets are proposed to be due to the polymer network structure. The integration of epoxy monomer crystals in PT10 inevitably results in an epoxy deficient thermoset formulation due to a significant number of epoxy functional groups being unavailable for reaction when in the crystal form. This results in a polymer network with naturally lower cross-linking density compared to the thermoset without integrated crystals, PT. Because the earlier stages of kinetics for *m/z* 182 are heavily influenced by the partially bound monomer mechanism proposed earlier, the resulting kinetics at this stage will also

be influenced by the polymer network cross-linking density and void content. This is because in order to detect the partially bound monomer product it must first migrate through the polymer network via thermal desorption. In the case of PT, this polymer network will have higher cross-linking density and result in higher in $E_{a,}$ while for PT10 the cross-linking density will naturally be lower and allow for easier migration of this product through the network, in turn lowering the E_a.

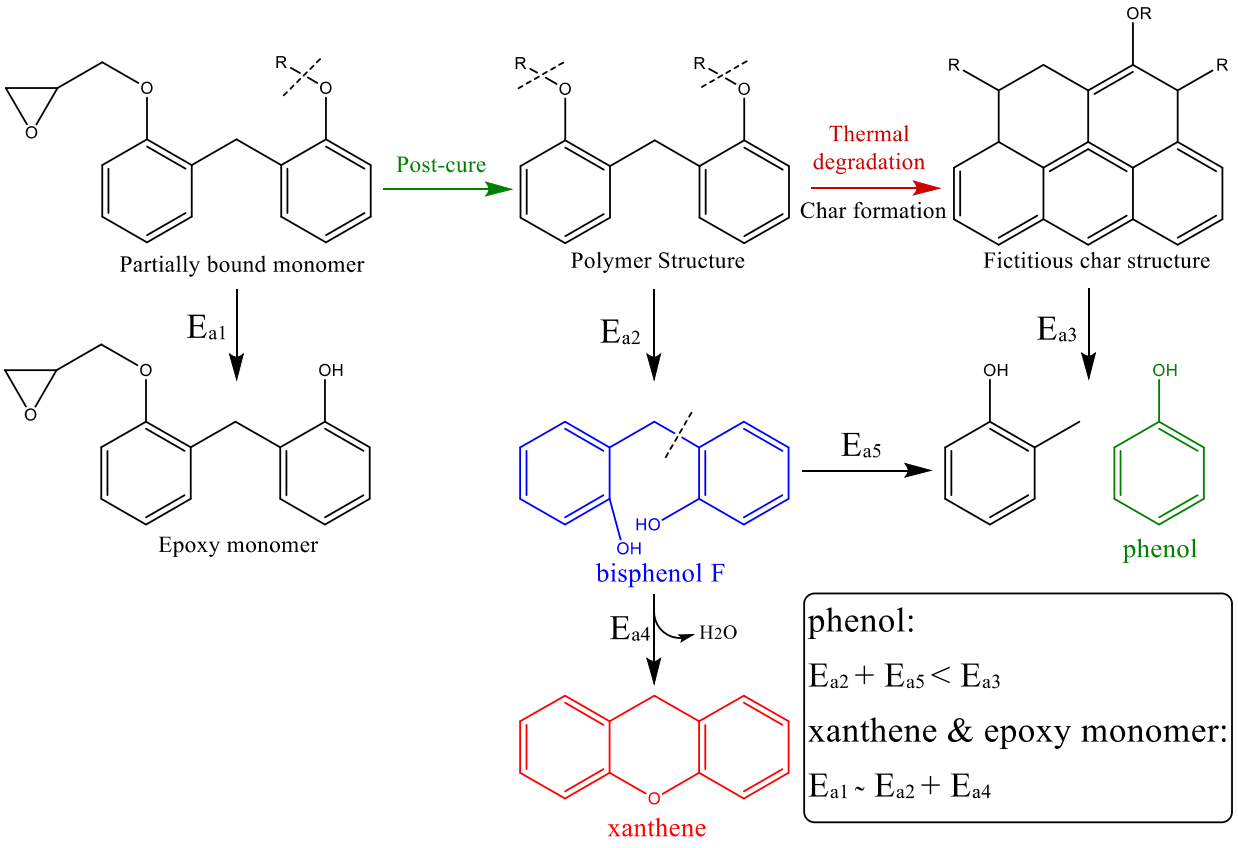

Figure 20. Proposed mechanism of epoxy monomer, bisphenol F, xanthene, and phenol formation with qualitative comparisons of activation energy.

4. CONCLUSION

In this work, we investigated the impact of integrating epoxy monomer crystals on the degradation kinetics of the resulting thermoset. Evolved gas analysis-MS coupled with product specific kinetics (PSK) analysis were utilized to obtained detailed information on the degradation kinetics of the thermosets. Integration of epoxy crystals was found to have minimal impact on the PSK of bisphenol F and xanthene products with the most significant impact on the phenol product. Specifically, integration of epoxy crystals appears to inhibit increases in E_a at later extent conversions after post-cure annealing which are seen in the thermoset without crystal inclusions. Phenol, at these later conversions, is hypothesized to come from degradation of newly formed char material; therefore, crystal integration impacts char formation. A new product was also identified in this work: a bisphenol F monomer with an epoxy functional group. This product shares the *m/z* 182 ion thought to be unique to xanthene but only forms in the lower temperature region of the thermographs typically associated with thermal desorption temperatures. This product was determined to be a result of a partially bound monomer and could potentially be used as an indicator of cure extent in the thermoset.

In conclusion, integration of crystalized epoxy monomers into prepolymer thermoset formulations has a significant impact on the degradation kinetics of the resulting thermosets. The level of detail provided in this work from PSK analysis is impossible to observe with typical TGA methods and further confirms that EGA-MS coupled with PSK analysis is a powerful complimentary technique to TGA methods to study the complex thermal processes of polymer materials.

AUTHOR INFORMATION

Corresponding Author

*Derek B. Dwyer—Oak Ridge National Laboratory, P.O. Box 2008 MS-6117, Oak Ridge, TN 37831; Email: dwyerdb@ornl.gov

ASSOCIATED CONTENT

Kinetics plots of the full mass spectra scans for both post cured thermosets, and conversion extent and kinetic plots for the product Ions phenol (*m/z* 66), xanthene (*m/z* 182), and bisphenol F isomers (*m/z* 200) (DOC)

REFERENCES

1. Desimoni, E.; Casella, G. I.; Salvi, A. M., XPS XAES STUDY OF CARBON-FIBERS DURING THERMAL ANNEALING UNDER UHV CONDITIONS. *Carbon* **1992,** *30* (4), 521-526.
2. Gupta, V.; Mathur, R. B.; Bahl, O. P.; Tressaud, A.; Flandrois, S., THERMAL-STABILITY OF FLUORINE-INTERCALATED CARBON-FIBERS. *Synthetic Metals* **1995,** *73* (1), 69-75.
3. Farsani, R. E.; Shokuhfar, A.; Sedghi, A., Fabrication of carbon fibres from wet-spun commercial polyacrylonitrile fibres. *Fibre Chemistry* **2006,** *38* (5), 383-386.
4. Goodhew, P. J.; Clarke, A. J.; Bailey, J. E., REVIEW OF FABRICATION AND PROPERTIES OF CARBON-FIBERS. *Materials Science and Engineering* **1975,** *17* (1), 3-30.
5. Li, H.; Wang, N. S. D.; Han, X. F.; Yuan, H. R.; Xie, J., Mechanism Identification and Kinetics Analysis of Thermal Degradation for Carbon Fiber/Epoxy Resin. *Polymers* **2021,** *13* (4).
6. Corres, M. A.; Zubitur, M.; Cortazar, M.; Mugica, A., Thermal and thermo-oxidative degradation of poly(hydroxy ether of bisphenol-A) studied by TGA/FTIR and TGA/MS. *J. Anal. Appl. Pyrolysis* **2011,** *92* (2), 407-416.
7. Grassie, N.; Guy, M. I.; Tennent, N. H., DEGRADATION OF EPOXY POLYMERS .4. THERMAL-DEGRADATION OF BISPHENOL-A DIGLYCIDYL ETHER CURED WITH ETHYLENE DIAMINE. *Polymer Degradation and Stability* **1986,** *14* (2), 125-137.
8. Campbell, C. G.; Astorga, D. J.; Duemichen, E.; Celina, M., Thermoset materials characterization by thermal desorption or pyrolysis based gas chromatography-mass spectrometry methods. *Polymer Degradation and Stability* **2020,** *174*.
9. Dwyer, D. B.; Isbill, S. B.; Niedziela, J. L.; Kapsimalis, R. J.; Duckworth, D. C., Influence of Temperature on Accessible Pyrolysis Pathways of Homopolymerized Bishphenol A/F Epoxies and Copolymers. *J. Anal. Appl. Pyrolysis* **2021,** *153*, 104978.
10. Dwyer, D. B.; Gallego, N. C.; Niedziela, J. L.; Kapsimalis, R. J.; Duckworth, D. C., Product Specific Thermal Degradation Kinetics of Bisphenol F Epoxy in Inert and Oxidative Atmospheres using Evolved Gas Analysis-Mass Spectrometry. *J. Anal. Appl. Pyrolysis* **2022,** *165*.
11. Brnardic, I.; Macan, J.; Ivankovic, H.; Ivankovic, M., Thermal degradation kinetics of epoxy/organically modified montmorillonite nanocomposites. *J. Appl. Polym. Sci.* **2008,** *107* (3), 1932-1938.
12. Zhou, S.; Chen, Z. G.; Tusiime, R.; Cheng, C.; Sun, Z. Y.; Xu, L.; Liu, Y.; Jiang, M. Q.; Zhou, J. L.; Zhang, H.; Yu, M. H., Highly improving the mechanical and thermal properties of epoxy resin via blending with polyetherketone cardo. *Composites Communications* **2019,** *13*, 80-84.

13. Cheng, Z. P.; Fang, M. H.; Chen, X. X.; Zhang, Y. T.; Wang, Y. X.; Li, H. J.; Qian, J., Thermal Stability and Flame Retardancy of a Cured Trifunctional Epoxy Resin with the Synergistic Effects of Silicon/Titanium. *Acs Omega* **2020,** *5* (8), 4200-4212.
14. Salasinska, K.; Barczewski, M.; Borucka, M.; Gorny, R. L.; Kozikowski, P.; Celinski, M.; Gajek, A., Thermal Stability, Fire and Smoke Behaviour of Epoxy Composites Modified with Plant Waste Fillers. *Polymers* **2019,** *11* (8).
15. Tarrio-Saavedra, J.; Lopez-Beceiro, J.; Naya, S.; Artiaga, R., Effect of silica content on thermal stability of fumed silica/epoxy composites. *Polymer Degradation and Stability* **2008,** *93* (12), 2133-2137.
16. Yang, G. J.; Heo, Y. J.; Park, S. J., Effect of Morphology of Calcium Carbonate on Toughness Behavior and Thermal Stability of Epoxy-Based Composites. *Processes* **2019,** *7* (4).
17. Safety Data Sheet obtained from Sigma-Aldrich [Online]; Bisphenol F diglycidyl ether; CAS No. 2095-03-6, https://www.sigmaaldrich.com/US/en/sds/sial/18443.
18. Safety Data Sheet obtained from Sigma-Aldrich [Online]; Bisphenol A diglycidyl ether; CAS No. 1675-54-3, https://www.sigmaaldrich.com/US/en/sds/sigma/d3415.
19. Morgan, R. J.; Oneal, J. E., EFFECT OF EPOXY MONOMER CRYSTALLIZATION AND CURE CONDITIONS ON PHYSICAL STRUCTURE, FRACTURE TOPOGRAPHY, AND MECHANICAL RESPONSE OF POLYAMIDE-CURED BISPHENOL-A-DIGLYCIDYL ETHER EPOXIES. *J. Macromol. Sci.-Phys.* **1978,** *B15* (1), 139-169.
20. Yang, X. T.; Zhu, J. H.; Yang, D.; Zhang, J. L.; Guo, Y. Q.; Zhong, X.; Kong, J.; Gu, J. W., High-efficiency improvement of thermal conductivities for epoxy composites from synthesized liquid crystal epoxy followed by doping BN fillers. *Compos. Pt. B-Eng.* **2020,** *185*.
21. Vincent, L.; Mija, A.; Sbirrazzuoli, N., Liquid crystalline and isotropic epoxy thermosets: Mechanism and kinetics of non-isothermal degradation. *Polymer Degradation and Stability* **2007,** *92* (11), 2051-2057.
22. Carfagna, C.; Amendola, E.; Giamberini, M., LIQUID-CRYSTALLINE EPOXY-RESINS CONTAINING BINAPHTHYL GROUP AS RIGID BLOCK WITH ENHANCED THERMAL-STABILITY. *Macromolecular Chemistry and Physics* **1994,** *195* (7), 2307-2315.
23. Vyazovkin, S.; Burnham, A. K.; Criado, J. M.; Perez-Maqueda, L. A.; Popescu, C.; Sbirrazzuoli, N., ICTAC Kinetics Committee recommendations for performing kinetic computations on thermal analysis data. *Thermochim. Acta* **2011,** *520* (1-2), 1-19.
24. Vyazovkin, S., *Isoconversional Kinetics of Thermally Stimulated Processes*. Springer: 2015.
25. Vyazovkin, S.; Sbirrazzuoli, N., Isoconversional Kinetic Analysis of Thermally Stimulated Processes in Polymers. *Macromol. Rapid Commun.* **2006,** *27*, 1515-1532.
26. Chen, K. S.; Yeh, R. Z., Pyrolysis kinetics of epoxy resin in a nitrogen atmosphere. *Journal of Hazardous Materials* **1996,** *49*, 105-113.
27. Cui, H.-W.; Jiu, J.-T.; Sugahara, T.; Nagao, S.; Suganuma, K.; Uchida, H.; Schroder, K. A., Using the Friedman method to study the thermal degradation kinetics of photonically cured electrically conductive adhesives. *J Therm Anal Calorim* **2015,** *119*, 425-433.
28. Venkatesh, M.; Ravi, P.; Tewari, S. P., Isoconversional Kinetic Analysis of Decomposition of Nitroimidazoles: Friedman method vs Flynn−Wall−Ozawa Method. *The Journal of Physical Chemistry A* **2013,** *117*, 10162-10169.
29. Rochester, J. R.; Bolden, A. L., Bisphenol S and F: A Systematic Review and Comparison of the Hormonal Activity of Bisphenol A Substitutes. *Environmental Health Perspectives* **2015,** *123* (7), 643-650.
30. Kim, Y. M.; Han, T. U.; Hwang, B.; Lee, Y.; Watanabe, A.; Teramae, N.; Kim, S. S.; Park, Y. K.; Kim, S., New approach for the kinetic analysis of cellulose using EGA-MS. *Polymer Testing* **2017,** *60*, 12-17.
31. Akahira, T.; Sunose, T., Method of determining activation deterioration constant of electrical insulating materials. *Res Report Chiba Inst Technol (Sci Technol)* **1971,** *16*, 22-31.

32. Starink, M. J., The determination of activation energy from linear heating rate experiments: a comparison of the accuracy of isoconversion methods. *Thermochim. Acta* **2003,** *404* (1-2), 163-176.
33. Apra, E.; Bylaska, E. J.; de Jong, W. A.; Govind, N.; Kowalski, K.; Straatsma, T. P.; Valiev, M.; van Dam, H. J. J.; Alexeev, Y.; Anchell, J.; Anisimov, V.; Aquino, F. W.; Atta-Fynn, R.; Autschbach, J.; Bauman, N. P.; Becca, J. C.; Bernholdt, D. E.; Bhaskaran-Nair, K.; Bogatko, S.; Borowski, P.; Boschen, J.; Brabec, J.; Bruner, A.; Cauet, E.; Chen, Y.; Chuev, G. N.; Cramer, C. J.; Daily, J.; Deegan, M. J. O.; Dunning, T. H.; Dupuis, M.; Dyall, K. G.; Fann, G. I.; Fischer, S. A.; Fonari, A.; Fruchtl, H.; Gagliardi, L.; Garza, J.; Gawande, N.; Ghosh, S.; Glaesemann, K.; Gotz, A. W.; Hammond, J.; Helms, V.; Hermes, E. D.; Hirao, K.; Hirata, S.; Jacquelin, M.; Jensen, L.; Johnson, B. G.; Jonsson, H.; Kendall, R. A.; Klemm, M.; Kobayashi, R.; Konkov, V.; Krishnamoorthy, S.; Krishnan, M.; Lin, Z.; Lins, R. D.; Littlefield, R. J.; Logsdail, A. J.; Lopata, K.; Ma, W.; Marenich, A. V.; del Campo, J. M.; Mejia-Rodriguez, D.; Moore, J. E.; Mullin, J. M.; Nakajima, T.; Nascimento, D. R.; Nichols, J. A.; Nichols, P. J.; Nieplocha, J.; Otero-de-la-Roza, A.; Palmer, B.; Panyala, A.; Pirojsirikul, T.; Peng, B.; Peverati, R.; Pittner, J.; Pollack, L.; Richard, R. M.; Sadayappan, P.; Schatz, G. C.; Shelton, W. A.; Silverstein, D. W.; Smith, D. M. A.; Soares, T. A.; Song, D.; Swart, M.; Taylor, H. L.; Thomas, G. S.; Tipparaju, V.; Truhlar, D. G.; Tsemekhman, K.; Van Voorhis, T.; Vazquez-Mayagoitia, A.; Verma, P.; Villa, O.; Vishnu, A.; Vogiatzis, K. D.; Wang, D.; Weare, J. H.; Williamson, M. J.; Windus, T. L.; Wolinski, K.; Wong, A. T.; Wu, Q.; Yang, C.; Yu, Q.; Zacharias, M.; Zhang, Z.; Zhao, Y.; Harrison, R. J., NWChem: Past, present, and future. *Journal of Chemical Physics* **2020,** *152* (18).
34. Zhao, Y.; Truhlar, D. G., A new local density functional for main-group thermochemistry, transition metal bonding, thermochemical kinetics, and noncovalent interactions. *Journal of Chemical Physics* **2006,** *125* (19).
35. Dunning, T. H., GAUSSIAN-BASIS SETS FOR USE IN CORRELATED MOLECULAR CALCULATIONS .1. THE ATOMS BORON THROUGH NEON AND HYDROGEN. *Journal of Chemical Physics* **1989,** *90* (2), 1007-1023.
36. Grimme, S.; Antony, J.; Ehrlich, S.; Krieg, H., A consistent and accurate ab initio parametrization of density functional dispersion correction (DFT-D) for the 94 elements H-Pu. *Journal of Chemical Physics* **2010,** *132* (15).
37. Dwyer, D. B.; Isbill, S. B.; Brubaker, Z. E.; Keum, J. K.; Bras, W.; Niedziela, J. L., Thermally Induced Structural Transitions in Epoxy Thermoset Polymer Networks and Their Spectroscopic Responses. *ACS Appl. Polym. Mater.* **2023,** *5*, 5961-5971.
38. Knox, S. T.; Wright, A.; Cameron, C.; Fairclough, J. P. A., Structural Variation and Chemical Performance-A Study of the Effects of Chemical Structure upon Epoxy Network Chemical Performance. *ACS Appl. Polym. Mater.* **2021,** *3* (7), 3438-3445.
39. Shiono, A.; Hosaka, A.; Watanabe, C.; Teramae, N.; Nemoto, N.; Ohtani, H., Thermoanalytical characterization of polymers: A comparative study between thermogravimetry and evolved gas analysis using a temperature-programmable pyrolyzer. *Polymer Testing* **2015,** *42*, 54-61.
40. Cohen, Y.; Aizenshtat, Z., INVESTIGATION OF PYROLYTICALLY PRODUCED CONDENSATES OF PHENOL FORMALDEHYDE RESINS, IN RELATION TO THEIR STRUCTURE AND DECOMPOSITION MECHANISM. *J. Anal. Appl. Pyrolysis* **1992,** *22* (3), 153-178.
41. Glockler, G., CARBON-OXYGEN BOND ENERGIES AND BOND DISTANCES. *Journal of Physical Chemistry* **1958,** *62* (9), 1049-1054.